THE UNIVERSITY OF MICHIGAN

INDUSTRY PROGRAM OF THE COLLEGE OF ENGINEERING

FREE CONVECTION HEAT TRANSFER AND FLUID FLOW IN CLOSED VESSELS WITH INTERNAL HEAT SOURCE

F. G. Hammitt
E. M. Brower
Paul T. Chu

November, 1959

IP-399

ACKNOWLEDGEMENTS

The authors would like to acknowledge the financial assistance of The University of Michigan Research Institute, the Chrysler Corporation and Atomic Power Development Associates in the work upon which this report is based. Also the assistance of the following students at this University is acknowledged: A. E. Brown, R. P. Hanson, and J. L. Summers.

TABLE OF CONTENTS

LIST OF TABLES

LIST OF FIGURES

Figure

LIST OF FIGURES (CONT'D)

LIST OF FIGURES (CONT'D)

Figure

NOMENCLATURE

T	Temperature
U	Dimensional velocity in axial position
u	Non-Dimensional velocity in axial direction = $\frac{a^2}{\kappa \ell} U$
X,x	Dimensional and non-dimensional coordinate in axial direction
R,r	Dimensional and non-dimensional coordinate in radial direction
ℓ,a	Length and radius of tube
ρ	Density
c_v	Specific heat
k	Thermal conductivity
κ	Thermal diffusivity, $\kappa = k/\rho c_v$
ν	Kinematic viscosity
A_s	Area of tube wall
t	Non-dimensional temperature $\frac{ga^4\Delta T}{\nu\kappa\ell}$; without subscript, non-dimensional temperature differential, wall to fluid, at any given axial position. Subscript o applies to differential between wall and centerline at top of tube. Subscript ℓ applies to differential between centerline at any given axial position and wall at bottom. Subscript ℓ_o applies to differential between centerline at top and wall at bottom. Subscript R applies to differential from wall fluid at any radius, r , and at any axial position.
t_w	Non-dimensional temperature differential between top and bottom of wall

$t_{\mathfrak{L}_o} = t_o + t_{w_o}$	Maximum non-dimensional temperature differential in the system = Ra . $\frac{a}{\ell}$
$t_{\mathfrak{L}}$	Non-dimensional temperature differential between fluid at centerline and wall at bottom
Ra_a	Rayleigh Number based on radius and maximum temperature differential $\frac{\alpha g a^3 (T_{wall_{min}} - T_{fluid_{max}})}{\nu\kappa}$
q_v	Non-dimensional volumetric heat source = $\frac{Q_v a^6 \alpha g}{p \nu \kappa^2 \ell c_v}$
Nu	Nusselt Number based on radius = $\frac{ha}{k}$
g	Acceleration of gravity
α	Coefficient of volumetric expansion
β	Non-dimensional core thickness 1-β is the non-dimensional boundary layer thickness and $\beta\mathfrak{R}$ is the radius at which the boundary layer is terminated. See Figure 20.
γ, γ', $F(\beta), G(\beta)$	Non-dimensional functions defined in text
h	Film coefficient for heat transfer

I. INTRODUCTION

The phenomenon of heat transfer and fluid flow under conditions of natural convection in a closed vessel wherein heat is generated as an internal heat source in the fluid and removed through an external coolant is of importance in the field of nuclear reactors and certain chemical processes. However, very little quantitative data is to be found in the literature regarding this phenomenon which will allow the design engineer to evaluate realistically the temperature differentials, fluid velocities, and wall heat flux distributions which are to be expected under a set of given physical conditions. It is the purpose of the research work herein reported to attempt to remedy this situation and to provide such engineering data.

Some of this work has been reported in previous research papers by the authors and co-workers at the University of Michigan.[1, 2, 3, 4, 5, 6] This report summarizes the previous papers and includes additional work performed subsequently.

Both experimental and analytical investigations are included. These cover a very large range of internal heat source strength, length to diameter ratio of the vessel, wall temperature and heat source distribution. They are limited to cases of axial symmetry in cylindrical vessels and to fluids of Prandtl Number near unity (i. e.: aqueous or gaseous fluids in general).

II. EXPERIMENTAL PROGRAM

A. Description of Facilities

The experimental data is derived from several pieces of apparatus which are similar in basic respects though differing somewhat in detail. In all cases heat is generated by ohmic resistance in an aqueous solution contained within a vertical, cylindrical, glass vessel; and removed to a coolant through the vessel walls. Heat loss through the vessel ends is essentially negligible. Temperature is measured within the fluid by a glass-encased thermocouple probe from which a small bead is exposed to the fluid. Velocities are estimated by timing the motion of dye or particles within the fluid.

The major portion of the data results from the water-cooled facility shown in Figures 1 and 2 and its subsequent modifications. Basically a cylindrical glass test section is held between carbon-steel electrodes at either end. It is surrounded by a larger plexiglass tube, forming an annulus

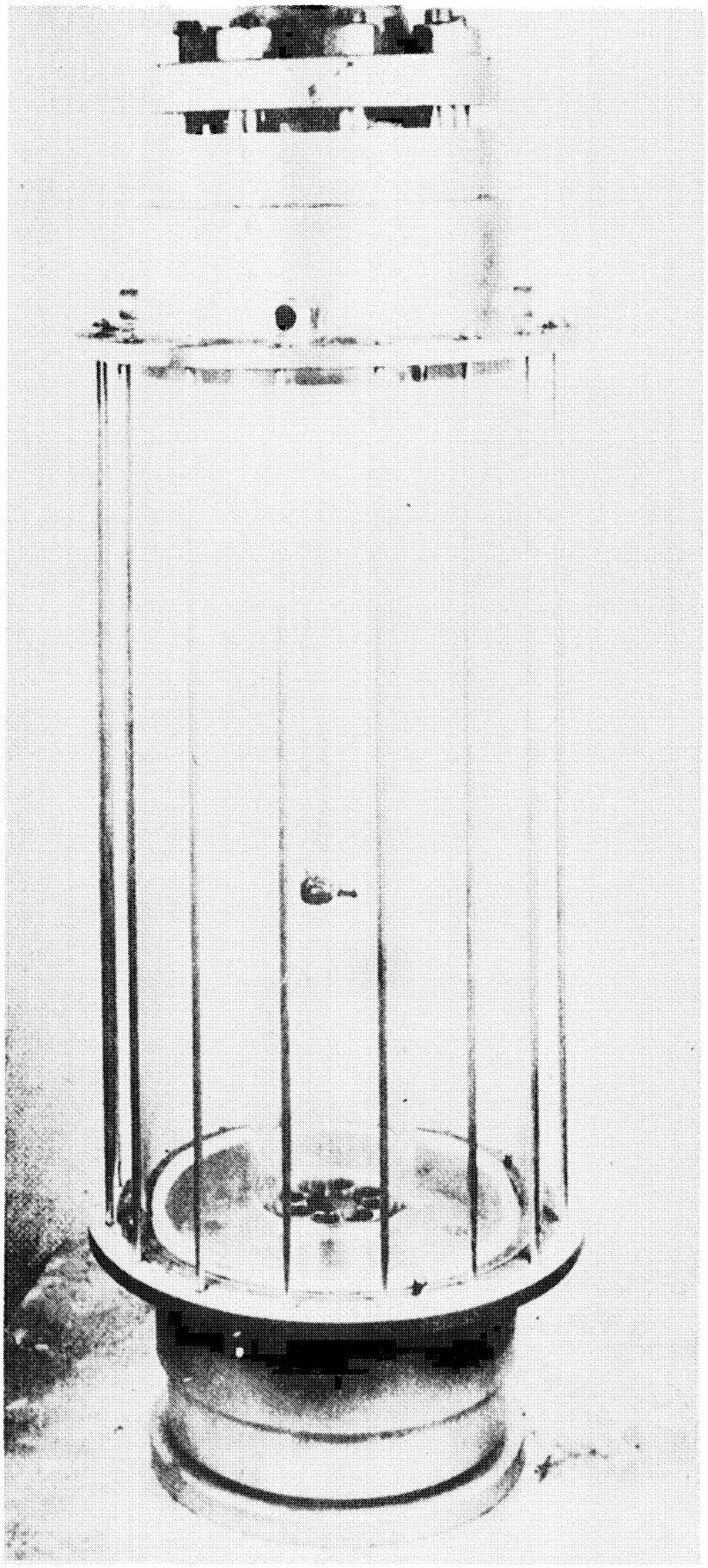

Figure 1. Photograph of Water Cooled Facility.

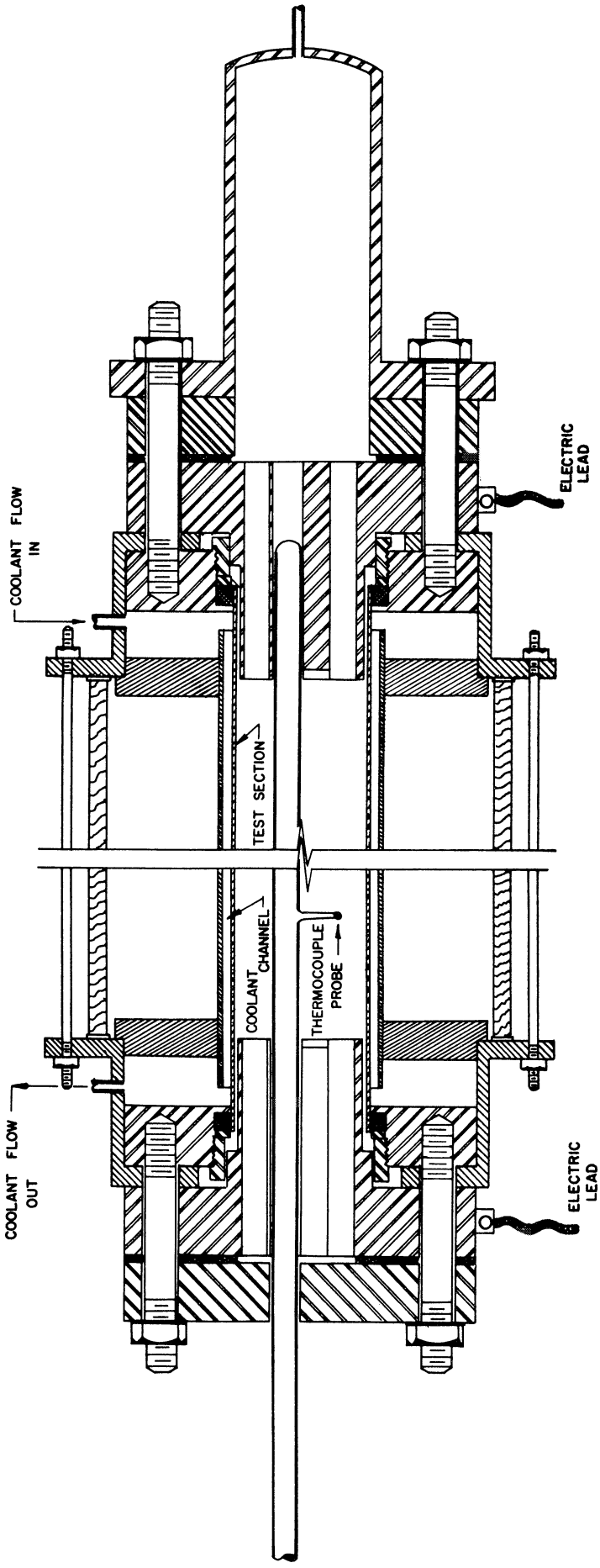

Figure 2. Layout Drawing of Water Cooled Facility.

for cooling water. The arrangement is such that test sections of various diameters and lengths can be used. In the tests conducted the length has been varied from 22-1/4 to 6-1/4 inches and the inside diameter from 3-7/8 to 7/8 inches, giving a range of length to diameter ratio from about 25 to about 1.6.

An eccentric vertical glass tube, guided by bushings in the electrodes, carries the thermocouple bead, measuring local fluid temperatures. It is capable of axial motion and rotation so that it may be positioned at any desired distance from the wall (except near the tube centerline) and at any desired axial position. Hence if axial symmetry is assumed it is possible to obtain a nearly complete temperature survey. The diameter of the eccentric thermocouple tube was approximately 20% of the test section inside diameter.

The independent variables which may be controlled with this facility are heat input rate, test section dimensions, and magnitude and direction of coolant flow. Power input could be measured most accurately electrically, but a check through a heat balance on the coolant was also used.

Two other slightly different facilities were used to obtain some of the test data. The first of these was identical in all major aspects to that described above except that the coolant was air in free convection rather than water in forced or free circulation. This arrangement was utilized initially because of its extreme simplicity.

The second variant arrangement differed from the others is that the vertical eccentric thermocouple was replaced by a multiplicity of glass thermocouple rods inserted through the sides of the vessel and capable of motion in the radial direction. This arrangement was used to investigate the validity of the assumption of axial symmetry which had been implicit in the other experimental and analytical work. Forced convection water cooling was used with this design and it was attempted to induce asymmetry of the internal flow by non-symmetrical cooling.

A final source of data was provided by several tests in a facility somewhat similar to that of Figures 1 and 2 (a thermocouple glass rod was extended from the top to reach any desired position by pivoting from the vessel top) which was used in tests at Oak Ridge described in Reference 4.

B. Experimental Results

1. General Applicability

The experimental data cover several categories which are listed below. All are presented in terms of non-dimensional parameters which are defined under Nomenclature. These are so constituted that the results are theoretically independent of length to diameter ratio.

a) Heat source strength vs. temperature differentials for various wall temperature distributions, magnitude and local direction.
b) Velocity vs. heat source strength.
c) Radial and axial temperature gradients as a function of heat source strength.
d) Wall heat flux distribution as a function of axial position and heat source strength.
e) Condition of turbulence as a function of heat source strength and temperature differentials.

The parameters of major importance are the non-dimensional heat source strength, q_v , and the non-dimensional temperature differentials, t . The overall heat transfer results of Figures 5, 6, 16, 21 and 22 are presented in terms of these two. The ratio, (maximum fluid to wall temperature differential) / (axial wall temperature differential), is used as the parameter to define a family of curves.

An examination of q_v discloses that it is proportional to the volumetric heat source strength / the vessel radius to the sixth power, and inversely to the vessel length.* Consequently a large volumetric heat source in a small-bore vessel is the equivalent of a much smaller volumetric heat source in a larger diameter vessel.

The non-dimensional temperature differential is actually a modified Rayleigh Number. It involves a grouping of dimensional and physical constants, which is that of the Rayleigh Number based on radius, multiplied by the radius to length ratio. In this report, the temperature differential used is defined by the subscript. The derivation on the various constants is explained further in the section under analytical results.

*It is also a function of various of the physical properties of the fluid.

2. Heat Source Strength vs. Temperature Differentials

The experimental data in all cases has been taken under conditions of apparent axial symmetry, but with the temperature of the wall adjacent to the test fluid falling from a maximum at the top of the test section to a minimum at the bottom. It is difficult to avoid a wall temperature gradient in this direction with the equipment used. For such a closed-end internal heat source cell, the wall heat flux (with uniform internal heat source) is a maximum at the top and minimum at the bottom. Hence the temperature differential across the wall decreases toward the bottom. When the outside wall temperature was maintained constant or even made to increase slightly toward the bottom by downward-flowing coolant, the effect of the wall temperature differntial was sufficient to give an inner wall gradient decreasing toward the bottom.

For a given physical configuration and heat source strength, the axial wall temperature gradient can be controlled by varying the coolant flow rate and direction. For most of the experiments, runs at a constant q_v, but varying coolant rate and direction were made so that points for a given q_v were attained for different axial wall temperature gradients. In some cases it was possible to obtain the same q_v with test sections of different length to diameter ratio. It was found that variation of this ratio within the limits of the experiments did not affect the results in terms of the non-dimensional parameters.

q_v depends not only on actual volumetric heat source and test section dimensions but also on the fluid physical properties which are functions of temperature. These were defined in relation to an average fluid temperature taken to be that measured on the vessel centerline at a point about 9/16 of the vessel length from the bottom. This point was selected asapproximately representative of the volume-averaged temperature.

In some cases q_v was not held entirely constant over a series of runs. In these cases it was prorated to the closest of the various fixed q_v values which had been used by assuming the validity of the relation between q_v and non-dimensional temperature differential derived analytically. The error so introduced should not be large since the prorated range is small.

The experimental points resulting from the above procedure are shown in Figures 3 and 4. The overall non-dimensional temperature differential* is plotted against the ratio of overall differential to

---

*Based on the differential between the fluid at the vessel centerline at the top and the wall at the bottom; i.e., the maximum differential existing.

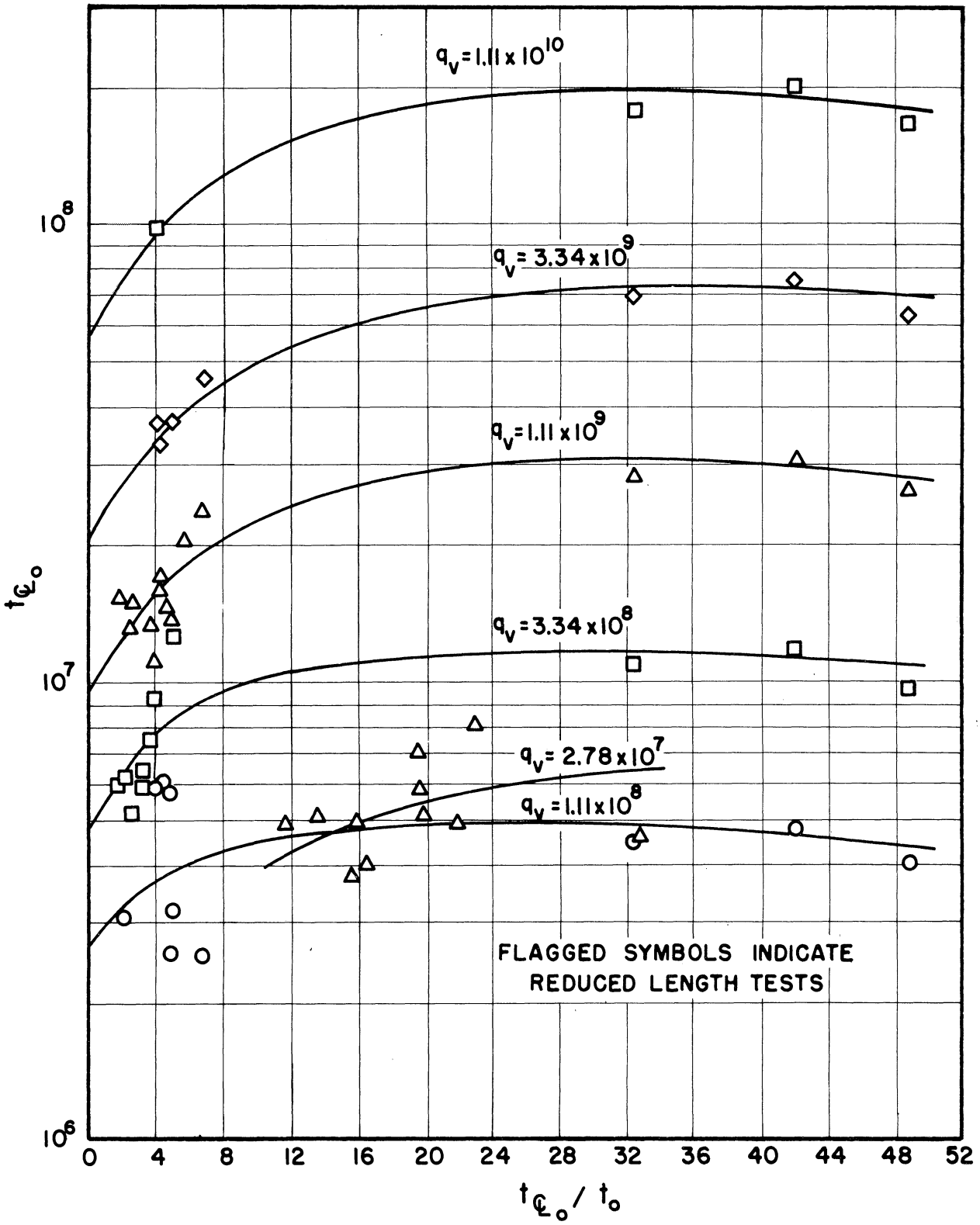

Figure 3. Non-Dimensional Overall Temperature vs. Overall/Radial Temperature Ratio, Experimental Data (High q_v Range).

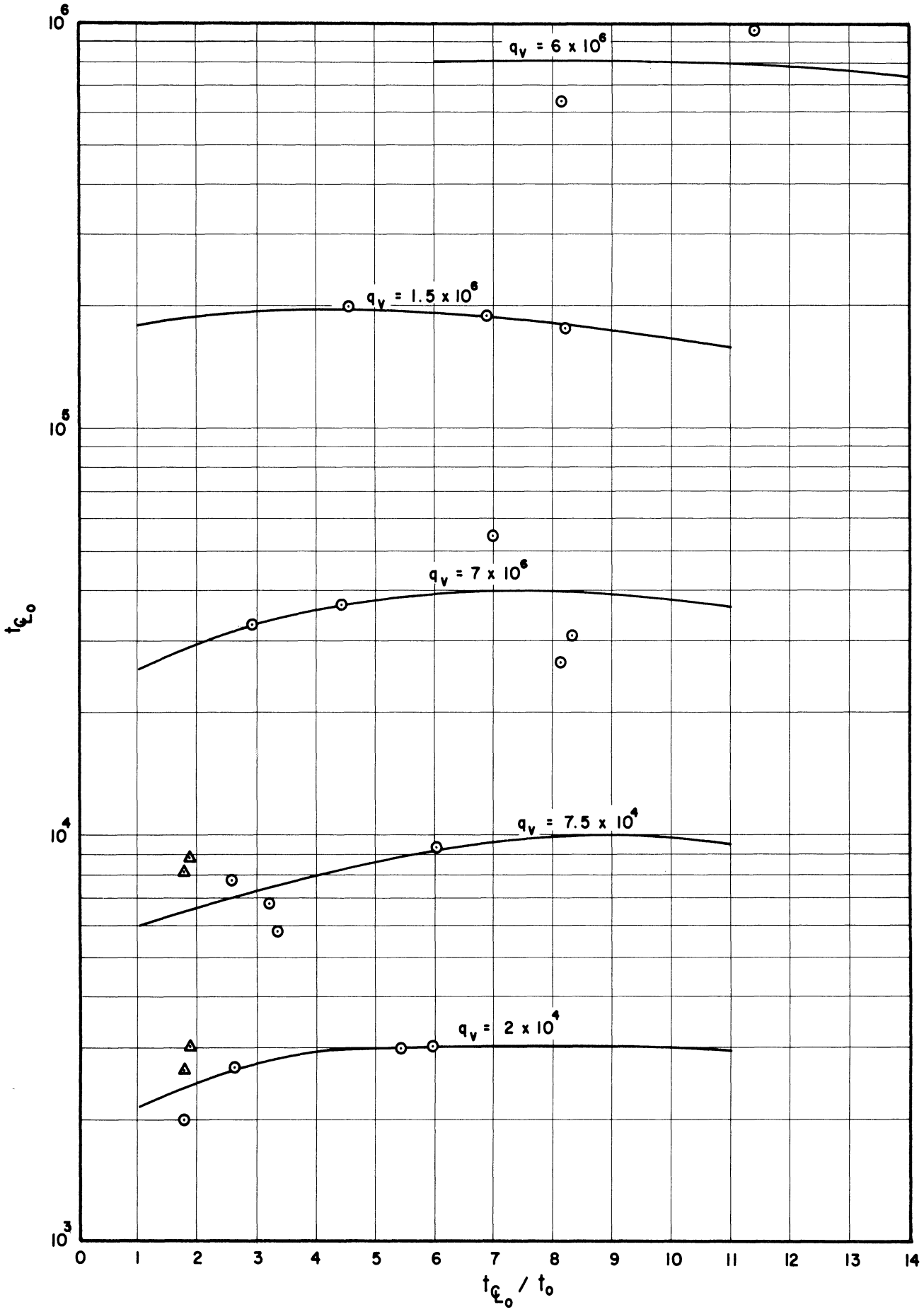

Figure 4. Non-Dimensional Overall Temperature vs. Overall/Radial Temperature Ratio, Experimental Data (Low q_V Range).

centerline-wall differential at the top* at the various q_v levels investigated. The q_v values range from approximately 10^{10} to 10^3.

The data of Figures 3 and 4 have been cross-plotted from the smoothed curves at values of the temperature ratio described above ranging from 1.0 to 20. Figure 5 is the resultant plot of q_v vs. t_{ℓ_o}. On logarithmic coordinates, this is a family of substantially straight lines with a slope ranging from approximately 1.3 for low q_v to 1.5 for higher q_v and low temperature ratios. Since a slope of about 1.24 is predicted by the laminar flow analysis, it is believed that these larger slopes are a result of more pronounced turbulent mixing as q_v is increased. A discontinuity in the curves is shown at q_v of about 10^6. It is believed that this is the result of rapidly increasing turbulent mixing in this area. However, since unfortunately there was no overlapping of data between the configuration producing the lower set of points and that producing the upper, adjacent to the discontinuity, it may be simply the result of experimental error resulting from slightly different measuring techniques.

As the temperature ratio is increased**, the overall temperature differential for a given q_v increases. This trend and the approximate magnitude of the shift agrees with the laminar flow analysis. Curves derived from the analysis for the corresponding conditions are shown in Figure 5 as dotted lines. It is noted that the experimental curves show a smaller temperature differential for a given heat source strength than the analysis predicts. Presumably this improved heat transfer is a result of the turbulent mixing which occurs to some extent in all the experiments but is not considered in the analysis. The improvement factor varies from about 1.2 for low q_v to about 1.5 for high q_v.

The calculated curves of Figure 5 are all based on a uniform wall temperature gradient whereas the experimental gradients were parabolic in nature (Figures 7,8,9 and 10). Calculations for a gradient typical of the experiments have been compared with those assuming uniform gradient. It was found that the effect on the overall temperature differential for a given q_v was small.

It was previously shown[1] that Nusselt's Number based on the radius is simply $q_v/2t$ where the temperature differential used in the calculation of the film coefficient is that corresponding to the non-dimensional temperature differential. Figure 6 is a plot of the experimental data showing Nusselt's Number versus q_v and is simply a cross-plot of the information of Figure 5.

---

*For constant wall temperature, this ratio is 1.0.

**This corresponds to proportionately greater wall temperature gradient.

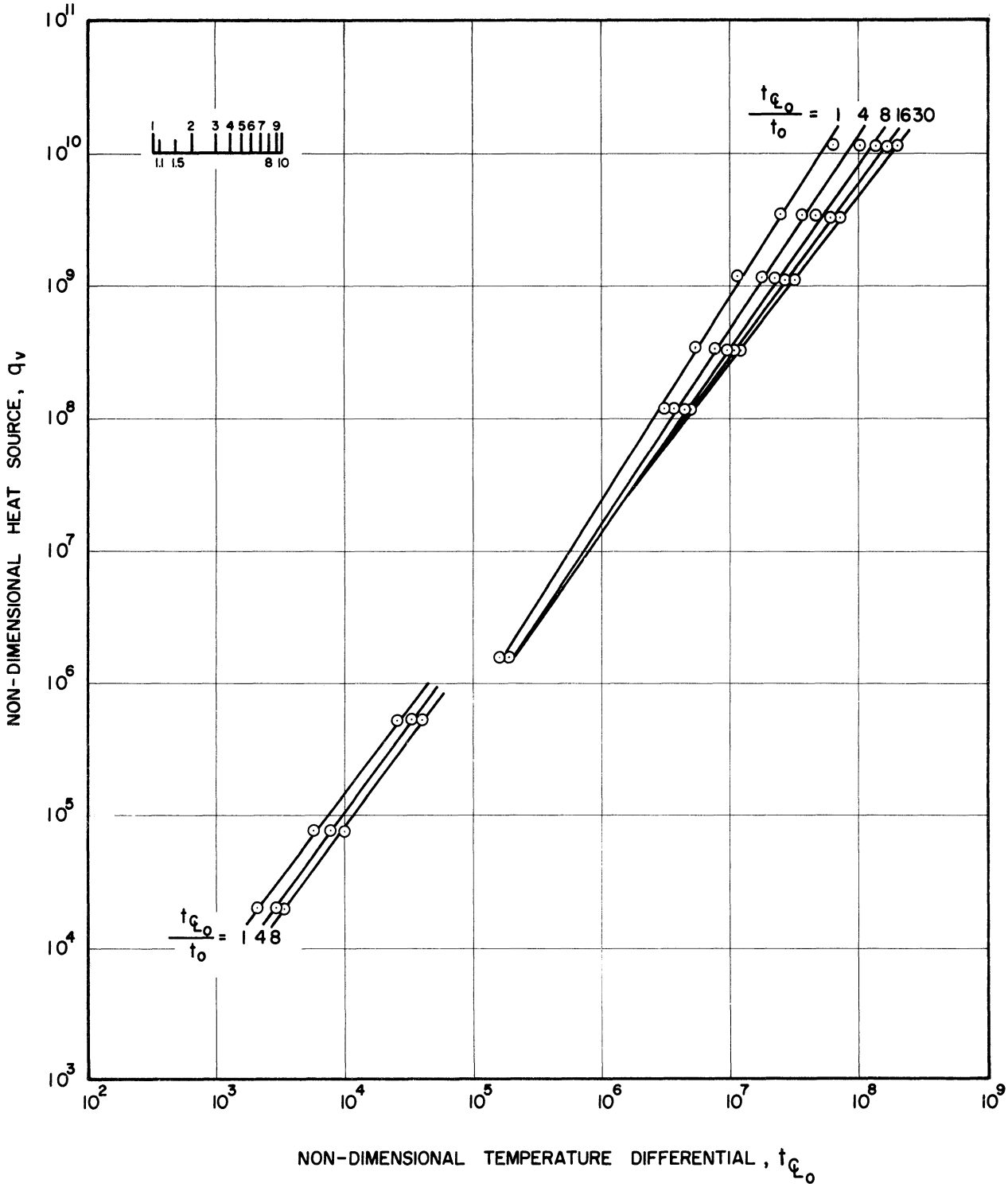

Figure 5. Non-Dimensional Heat Source, q_v, vs. Non-Dimensional Overall Temperature Differential, Experimental Data.

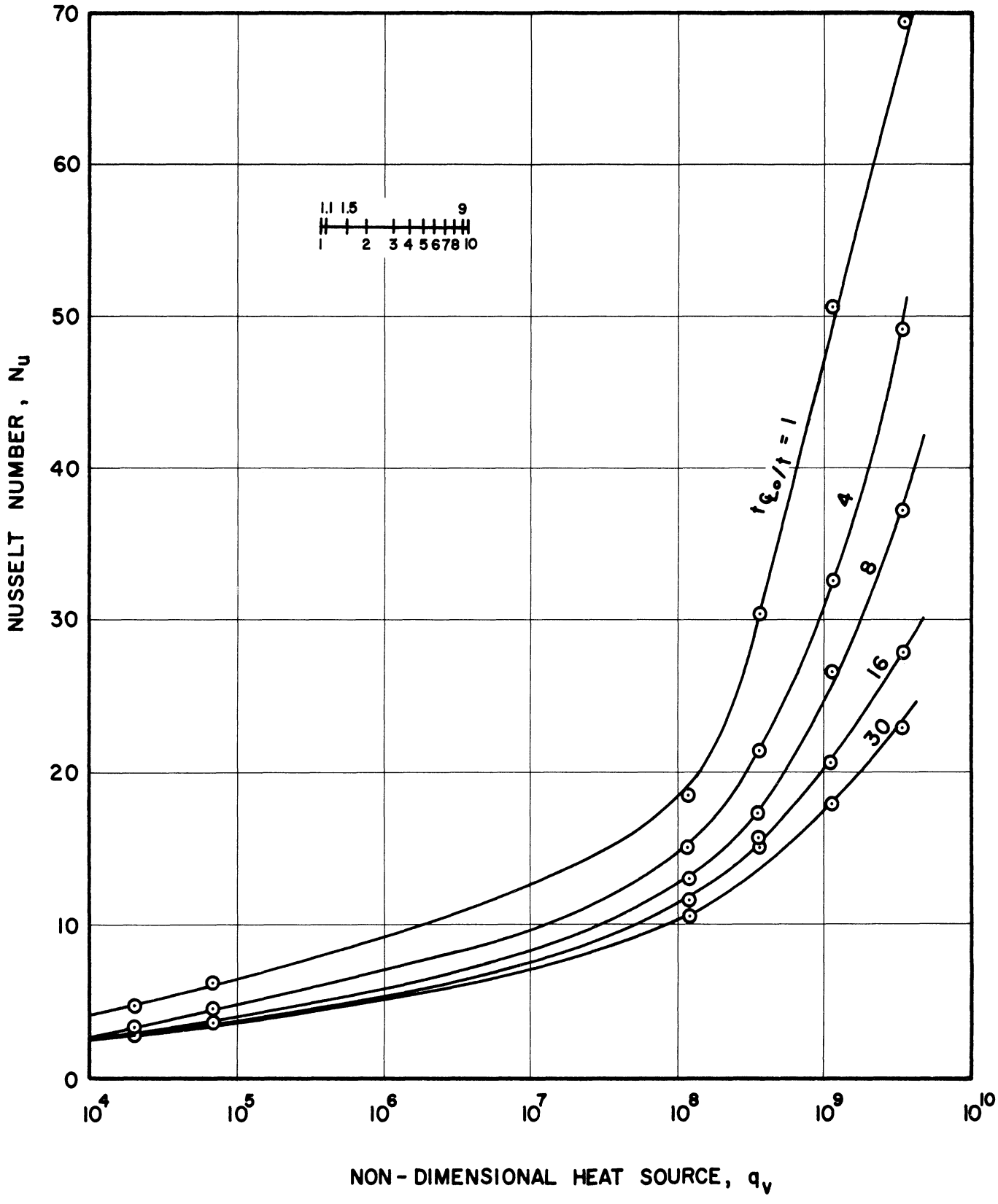

Figure 6. Non-Dimensional Heat Source, q_v, vs. Nusselt Number.

3. Axial Temperature Distribution

Figures 7, 8, 9, and 10, show the experimental axial wall and fluid centerline temperature distributions for the various q_v ranges. These curves are affected by the form and magnitude of the coolant flow. However, in general the wall temperature gradient is not uniform but increases rapidly toward the bottom. Also the differential between fluid centerline and wall at a given axial position is generally fairly constant in the upper part of the vessel and decreases rapidly toward the bottom. For similar wall temperature distribution this trend is predicted by the analysis.

4. Radial Temperature Gradient and Axial Symmetry

For the range of q_v studied, the analysis predicts a boundary layer type of flow pattern wherein the outer portion of fluid adjacent to the wall will descend and the inner portion, or core, ascend. The radial extent of the outer descending boundary layer will be small and at high q_v values (corresponding to most of the experimental range), but it will increase as q_v is reduced. A substantial upward velocity along the centerline is then required for the closed vessel. Since, over most of the range, the descending layer occupies only a small portion of the total area, the descending boundary layer velocity, will be greater than the ascending core velocity.

With such a boundary layer flow pattern it is to be expected on theoretical grounds[5, 6] that the radial temperature gradient will have approximately the same radial extent as the corresponding velocity gradient, and that the temperature will be approximately constant across the core at a given axial position.

These expected patterns have been observed. Figures 11, 12, 13, 14 and 15 show representative radial temperature profiles for widely spaced q_v values. As q_v is reduced the radial extent of the temperature gradient is increased as anticipated. The values agree approximately with the theoretical expectations.

With the exception of Figure 15, the above data were taken with the eccentric vertical thermocouple probe previously described. Hence points at varying distances from the wall are also taken at varying angular positions. Since the points taken with the eccentribe probe form a regular profile, there is a strong presumption that approximate axial symmetry must exist in these cases. It is the authors' opinion, based on their observations of the flow, that there is no significant variation from axial symmetry in these tests and that the effect of the probe is small. Its

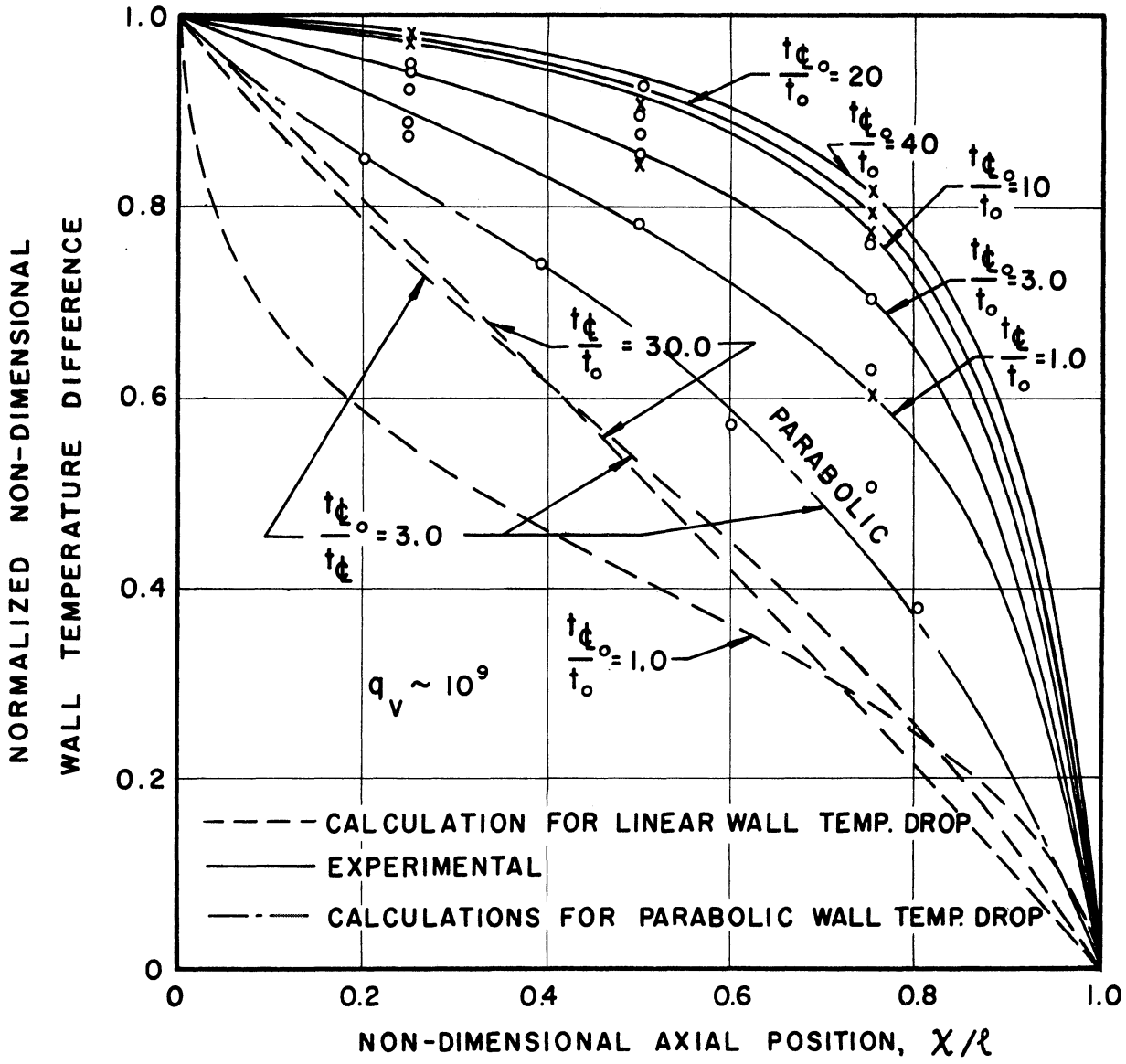

Figure 7. Non-Dimensional Centerline Temperature vs. Non-Dimensional Axial Position, Experimental Data Compare to Linear and Parabolic Wall Temperature Distribution, $q_v \ell \simeq 10^9$.

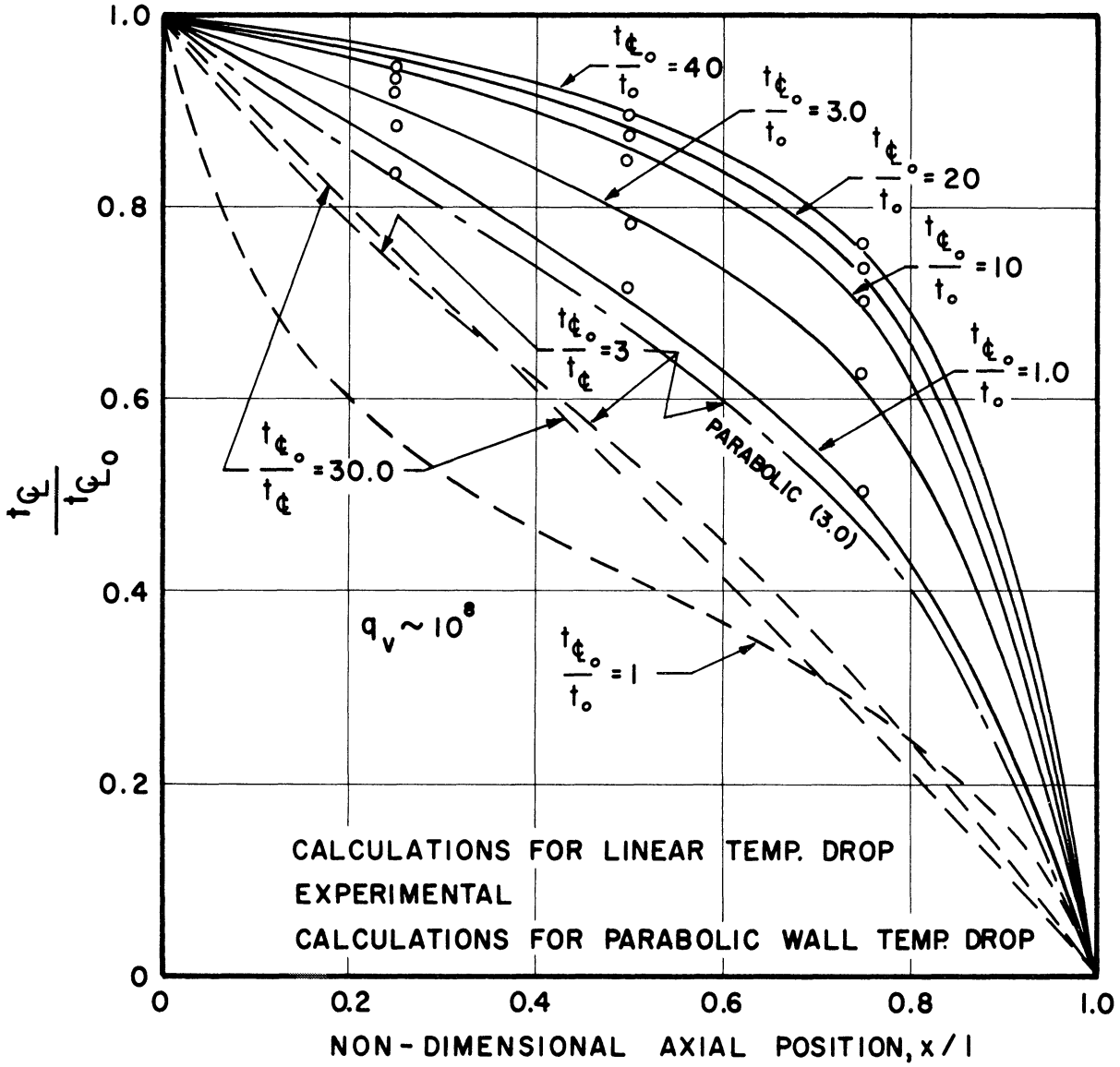

Figure 8. Non-Dimensional Centerline Temperature vs. Non-Dimensional Axial Position, Experimental Data, Compare to Linear and Parabolic Wall Temperature Distribution, $q_v \simeq 10^8$.

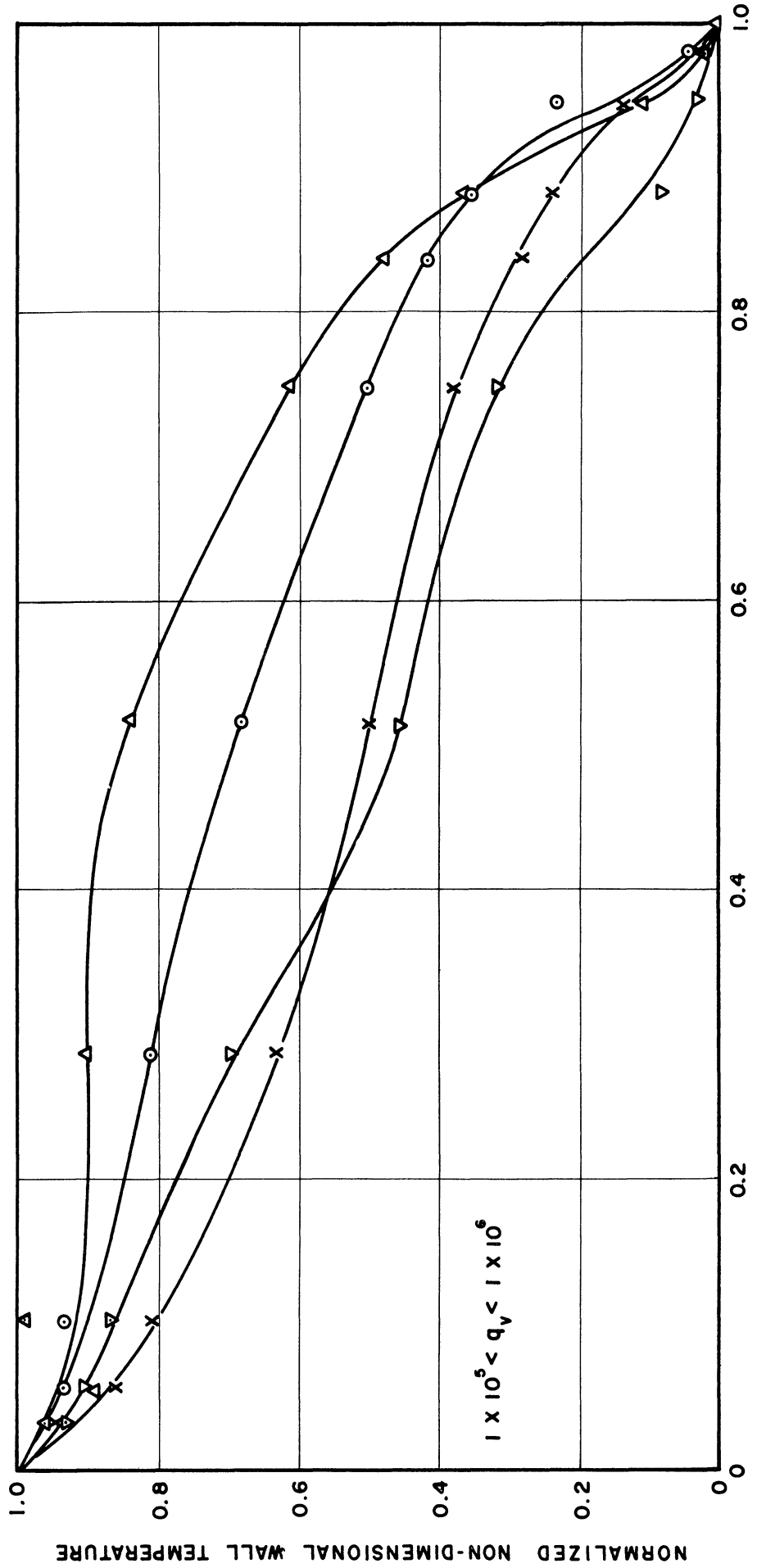

Figure 9. Non-Dimensional Centerline Temperature vs. Non-Dimensional Axial Position, Experimental Data, Compare to Linear and Parabolic Wall Temperature Distribution, $1 \times 10^5 < q_v < 1 \times 10^6$.

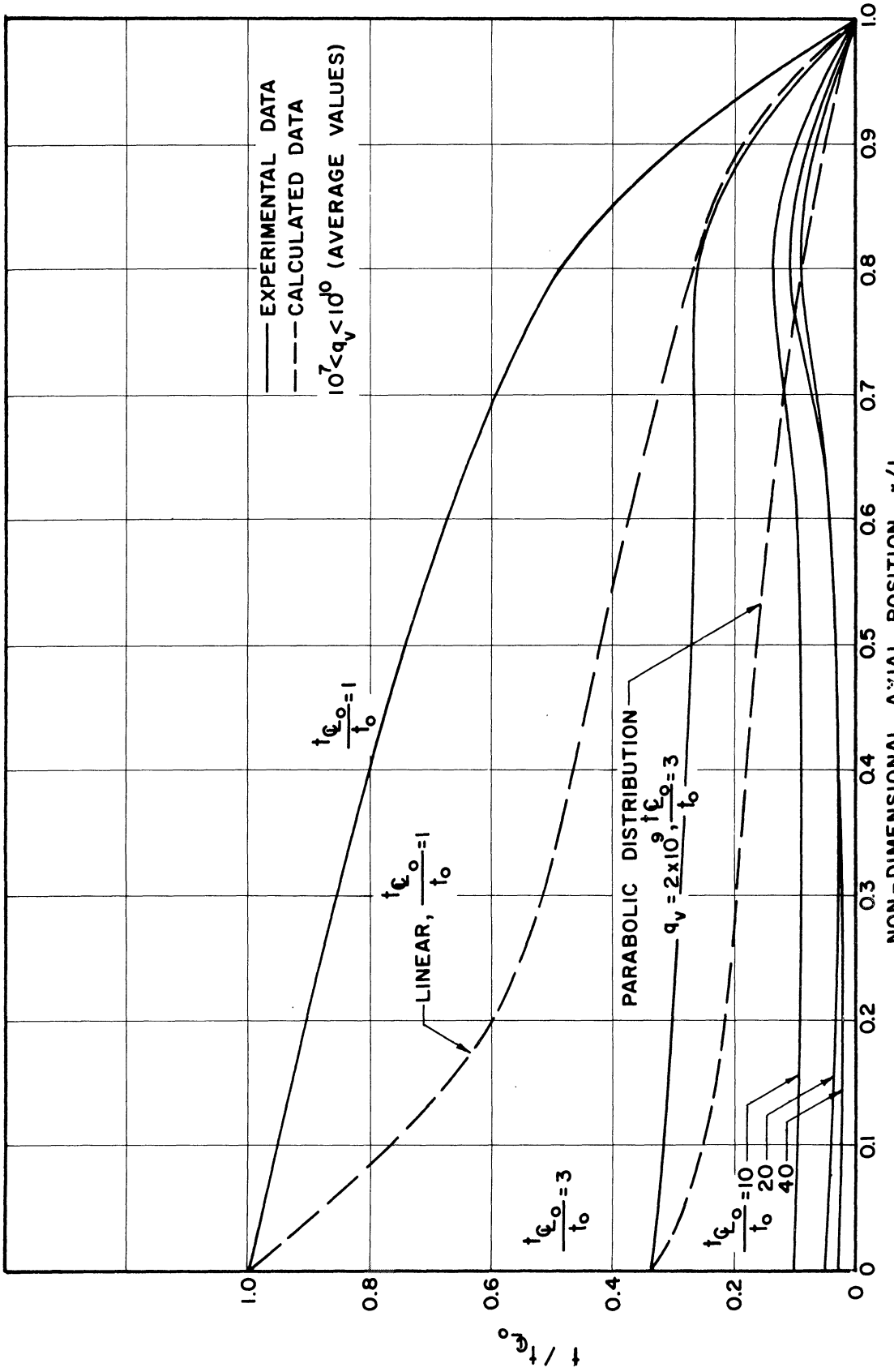

Figure 10. Non-Dimensional Temperature Differential Centerline to Wall vs. Axial Position.

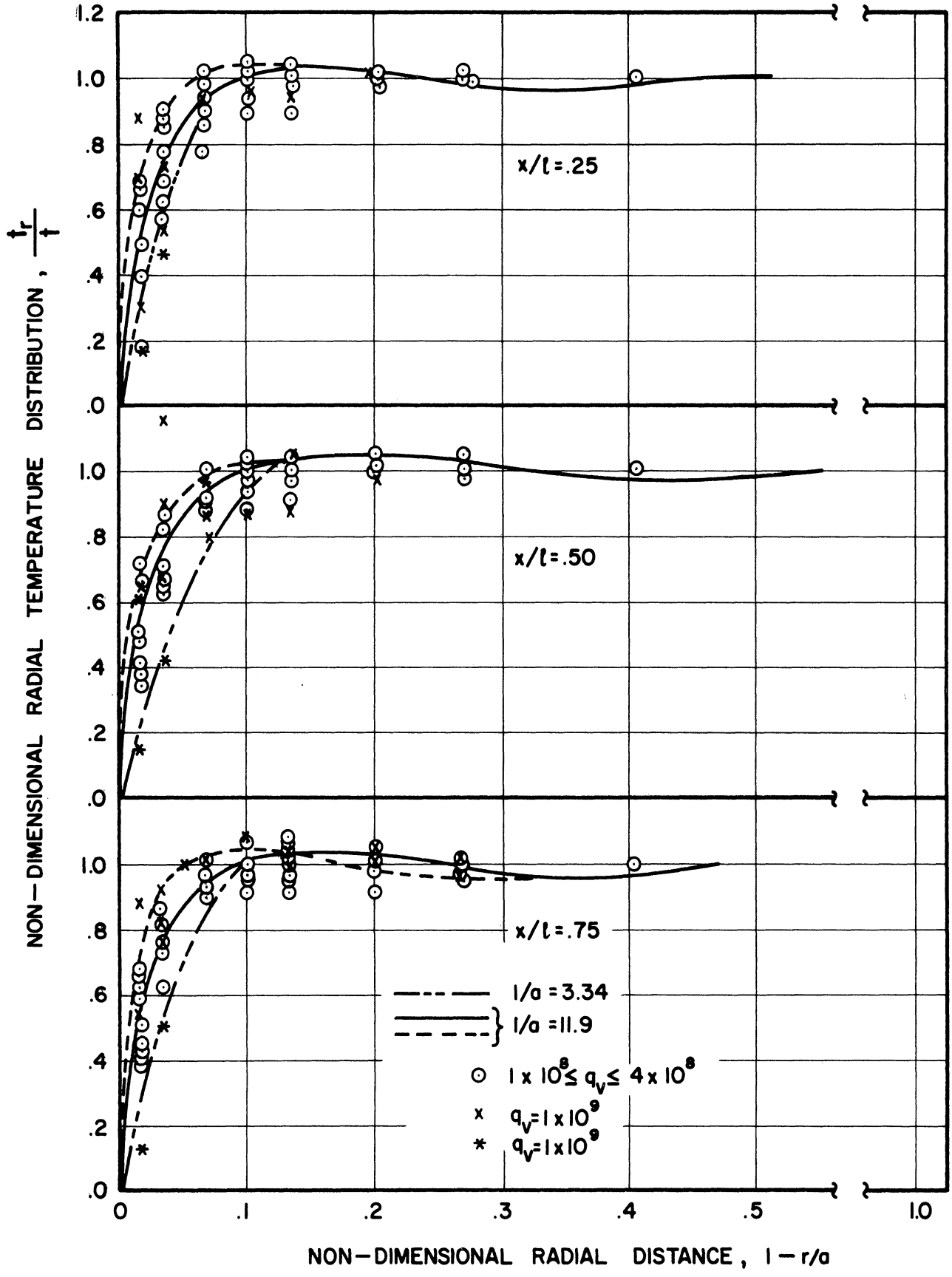

Figure 11. Non-Dimensional Radial Temperature Distribution vs. Radial Distance $q_v \geq 1 \times 10^8$.

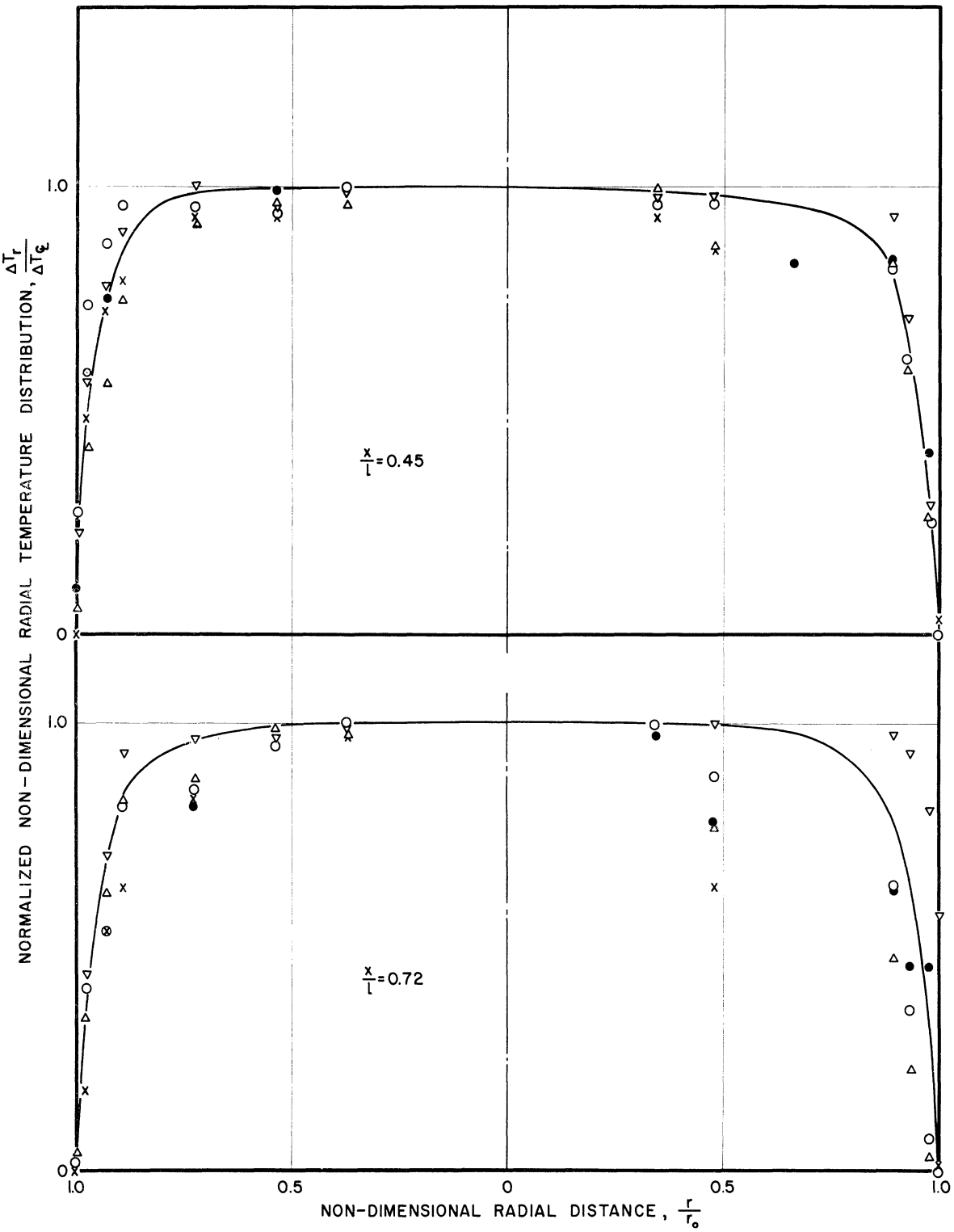

Figure 12. Non-Dimensional Radial Temperature Distribution vs. Radial Distance, $2 \times 10^5 \leq q_v \leq 1 \times 10^6$.

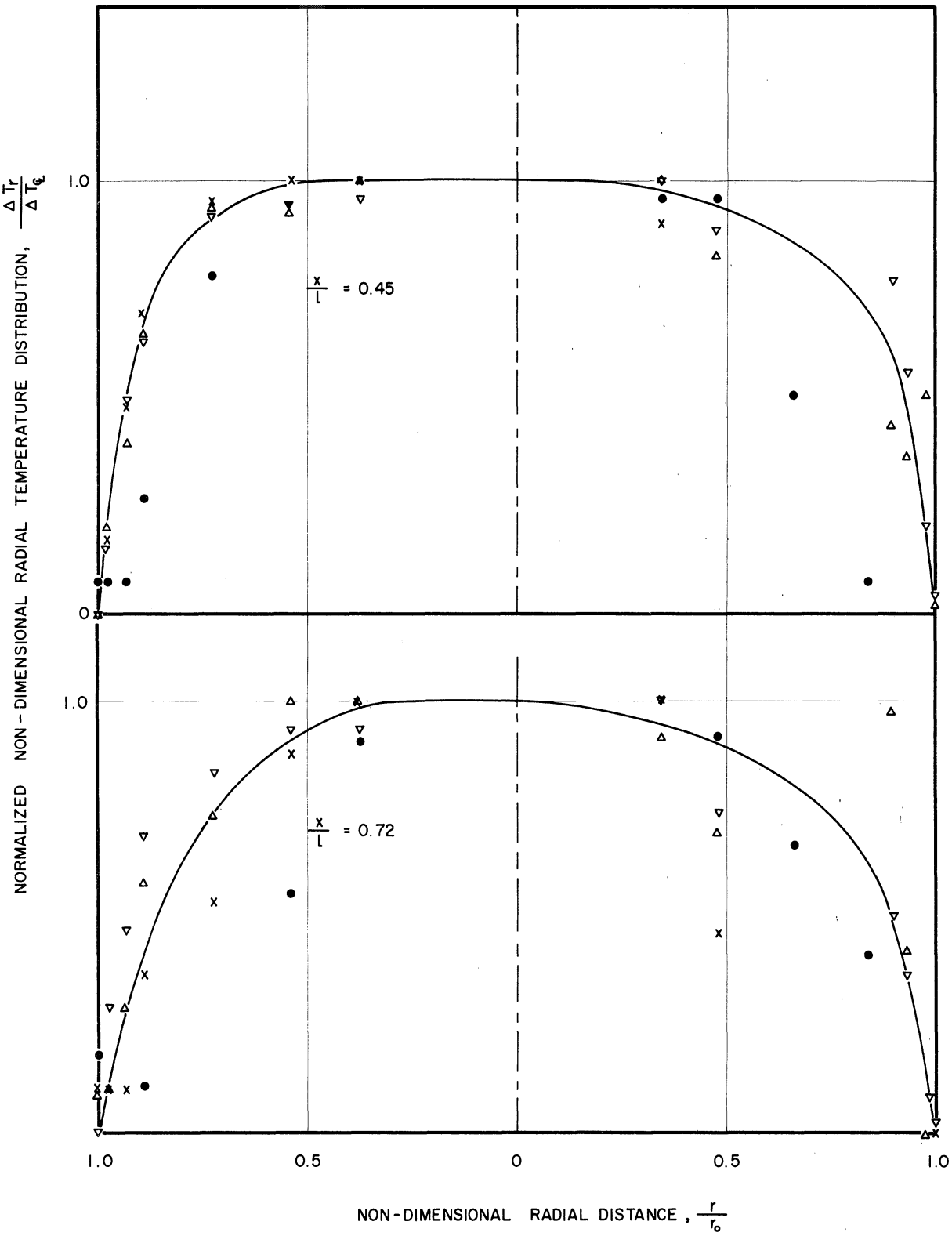

Figure 13. Non-Dimensional Radial Temperature Distribution vs. Radial Distance, $5 \times 10^4 \leq q_v \leq 1 \times 10^5$.

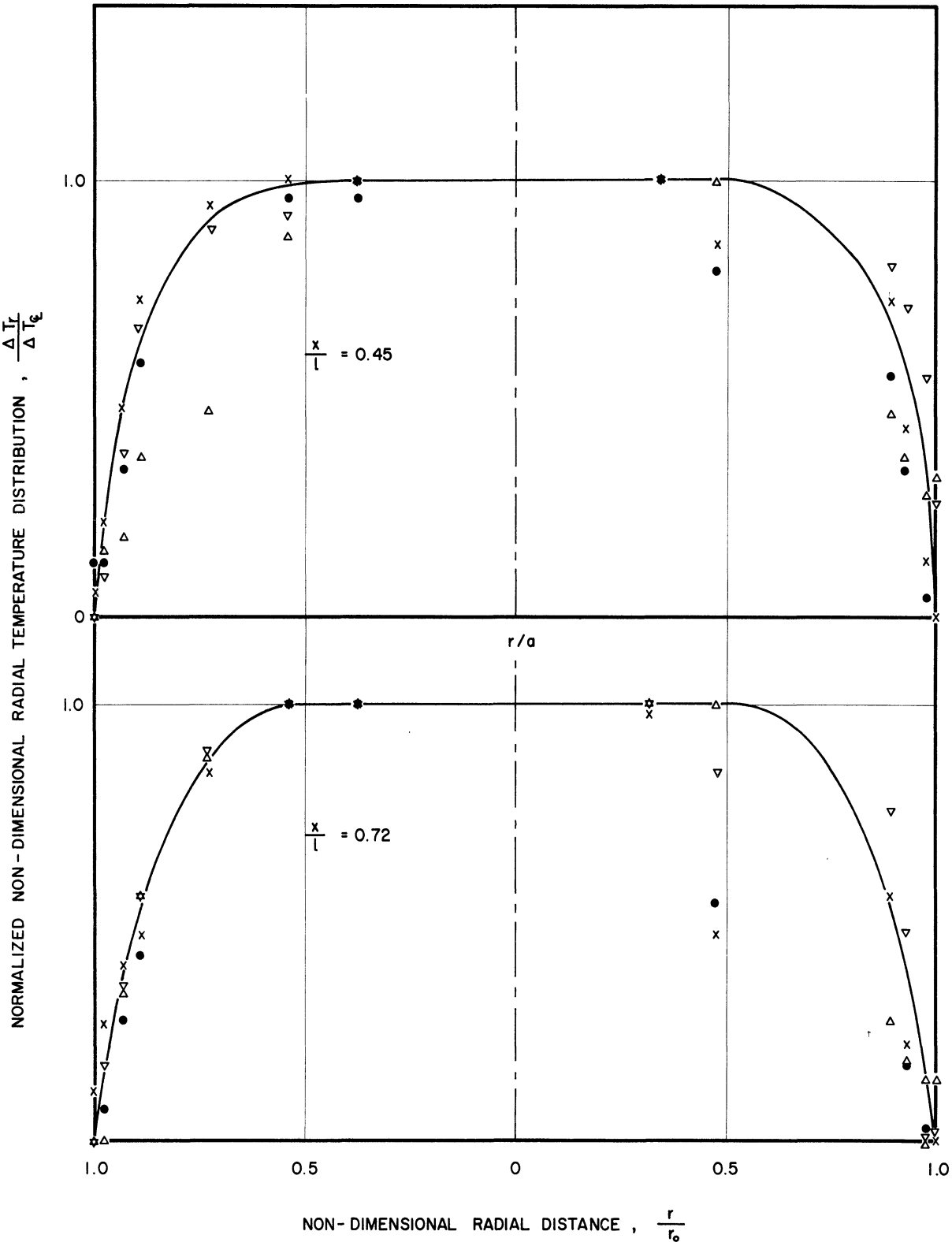

Figure 14. Non-Dimensional Radial Temperature Distribution vs. Radial Distance, $1 \times 10^4 \leq q_v \leq 4 \times 10^4$.

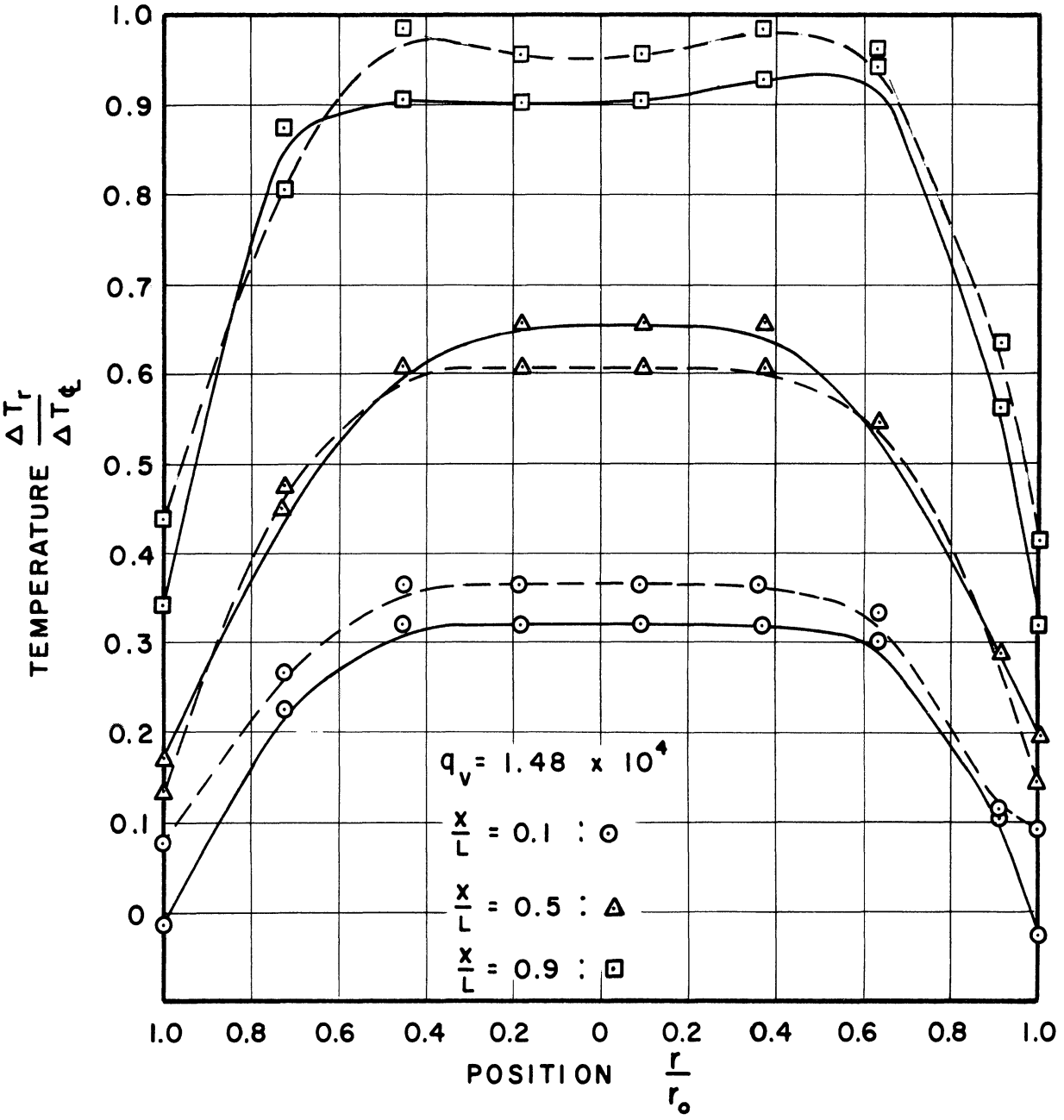

Figure 15. Non-Dimensional Radial Temperature Distribution vs. Radial Distance.

contribution to shear area is obviously small and exists in a region of low velocity. Also its share of cross-sectional area is extremely small.

The data of Figure 15 was taken from a facility wherein the temperature was measured by radial probes at various angles of rotation at a given axial position. Thus it was possible to measure the radial temperature profile at several angles of rotation and to check the existence of axial symmetry. In all cases it was found to exist within experimental accuracy although attempts were made to induce non-symmetry. This experiment was performed to induce a concentration of the downward velocity on one side of the vessel and upward on the other as reported for parallel flat plates.[9] However, such a result was not obtained. Full details are given in Reference 7.

An examination of the radial profile curves discloses that in many cases the temperature reaches a maximum at the juncture between the boundary layer and the core and then decreases at greater radii. It is believed that this is not simply experimental error since similar curves have been shown by other investigators. In an over-simplified manner the phenomenon can be explained by the fact that the fluid in this region is retarded in its motion and kept away from the cooling surfaces for a longer time than fluid traveling upward in the central portion of the vessel. However, heat is generated uniformly throughout the fluid, and conduction is almost negligible as a heat transfer mechanism throughout the body of the fluid.

5. Velocity and Boundary Layer Thickness Observation

Velocity observations were made visually. In some cases dye was injected at known locations, using an injector attached to the thermocouple probe, and its motion timed. It was possible to obtain a semi-quantitative indication of the velocity direction, magnitude, and state of turbulence at any point within the test section. In other cases the motion of particles within the fluid was timed, giving an approximate indication of the mean upward and downward velocity magnitudes.

It was found, as expected, that the interface between upward and downward flow was radially at approximately the same position as the inner extreme of the radial temperature gradient.

The experimentally observed maximum boundary layer and core velocities are plotted as a function of q_v in Figure 16. These are compared with the values derived from the laminar flow analysis. The observed boundary layer velocity is less than that expected and the core velocity is more.

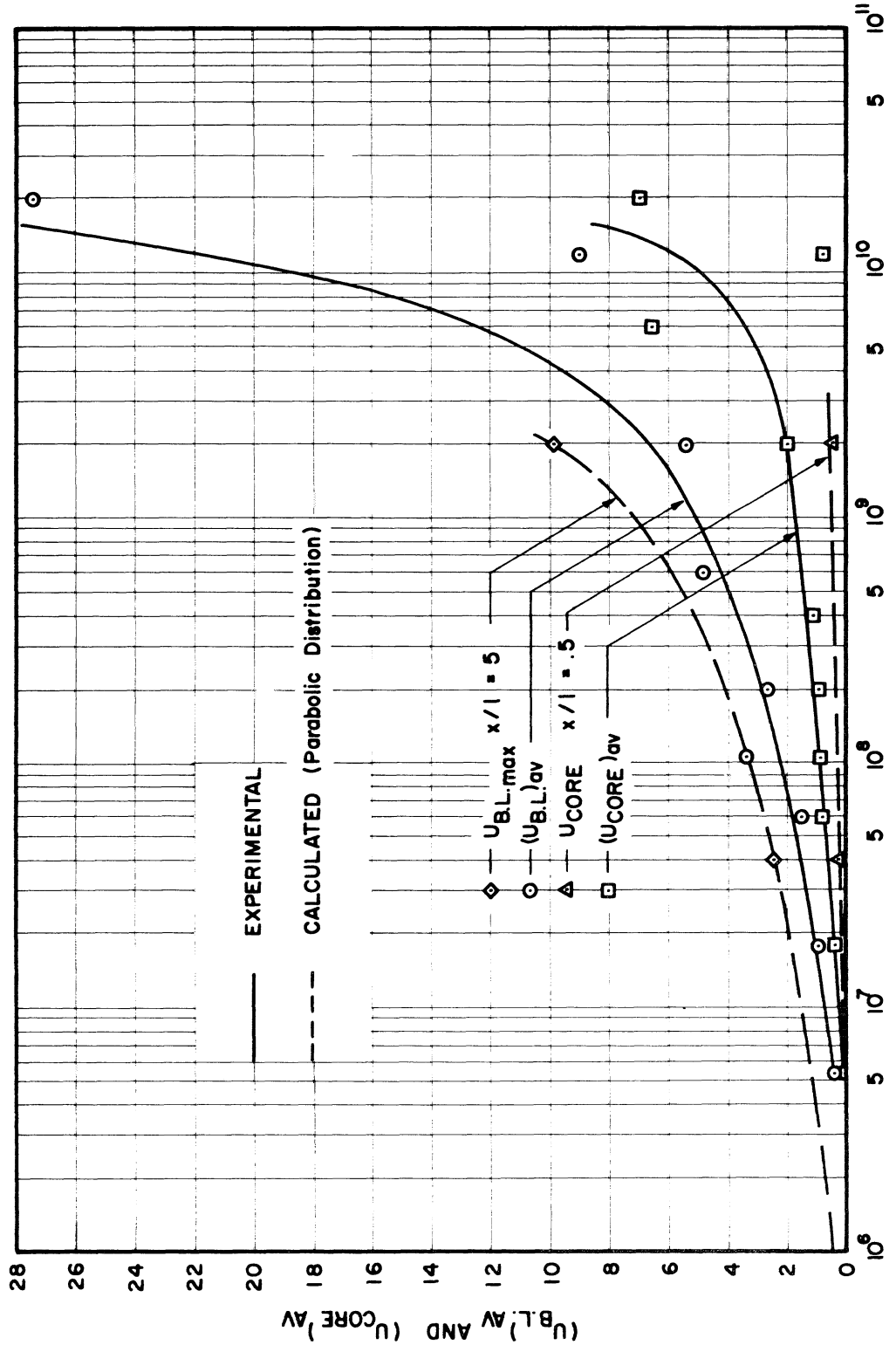

Figure 16. Non-Dimensional Boundary Layer and Core Velocity vs. Non-Dimensional Heat Source, Comparison of Experimental and Calculated Data.

Presumably, the retardation of the boundary layer velocity is a result of the turbulent mixing.

The boundary layer thickness from the radial temperature profile measurements is plotted as a function of q_v in Figure 17. It is noted that the thickness decreases with increasing q_v. A curve derived from the analysis is shown for comparison. Fair agreement exists.

6. Laminar-Turbulent Transition and Non-Steady State Effects

Observation of the flow discloses that truly laminar conditions did not apply to the entire vessel in any run except perhaps those tests conducted at the lowest q_v. The lack of laminar flow (perhaps small eddy is a better description) was evidenced in the dye tests and also by the fact that the local temperature readings fluctuated continually. Typically, the period of fluctuation was of the order of 15 to 30 seconds. However, the magnitude of the period may be due more to the characteristics of the precision potentiometer used than to the flow. Somewhat similar observations have been made in the past by other investigators.[10]

There is no abrupt change from laminar to turbulent flow in this configuration. Laminar conditions break down first in regions of high shear at the interface between upward and downward flow and, in general, in the upper rather than the lower portion of the vessel. Since the lower portion is relatively stagnent, laminar conditions persist here longest. Within the range of observations made, it appeared that in no case was the flow either entirely laminar or entirely turbulent. Rather laminar conditions were restricted to a larger or smaller portion of the vessel, including always the extreme lower portion.

The various experimental runs are listed in Table I in order of ascending Rayleigh Number based on the temperature differential from fluid centerline to wall across the top of the vessel radius. The division between substantially laminar conditions and substantially turbulent (i.e., where there is turbulent in perhaps 1/2 the vessel volume) occurs for a Rayleigh Number value so defined of about 4×10^7. This parameter appears more successful than either length Rayleigh Number or q_v in delineating the degree of turbulence. This is perhaps to be expected on theoretical grounds. However, considerably more basic research is required. Prediction is complicated by the closed loop nature of the flow leading to reappearance of general turbulence.

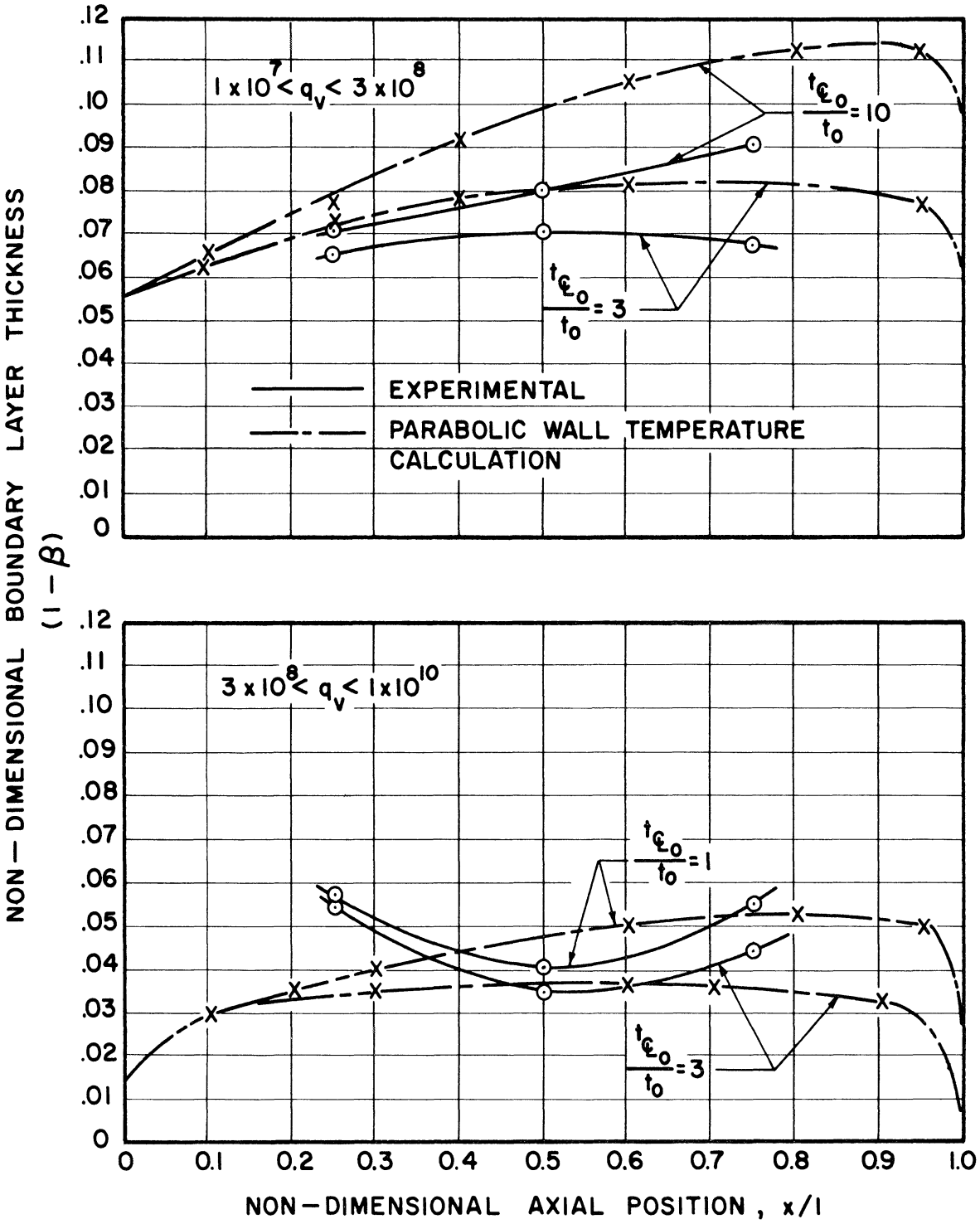

Figure 17. Non-Dimensional Boundary Layer Thickness vs. Non-Dimensional Axial Position.

TABLE I

LAMINAR-TURBULENT TRANSITION DATA

Ra_a	Ra_ℓ	q_v	Remarks
1.22×10^7	2.5×10^9	2.0×10^7	All laminar
1.28×10^7	4.44×10^{10}	5.4×10^6	All laminar
1.39×10^7	1.32×10^{10}	1.0×10^7	All laminar
1.72×10^7	6.66×10^8	6.0×10^8	Slight turbulence
2.00×10^7	7.79×10^8	2.0×10^8	No comment
2.06×10^7	4.17×10^9	4.2×10^7	All laminar
2.4×10^7	2.17×10^{10}	1.6×10^7	All laminar
2.89×10^7	1.0×10^{11}	1.7×10^7	No comment
3.00×10^7	5.05×10^{10}	2.0×10^8	No comment
3.05×10^7	5.11×10^{10}	2.0×10^8	No comment
3.28×10^7	6.66×10^9	5.9×10^7	All laminar
3.39×10^7	3.5×10^{10}	3.0×10^7	All laminar
3.56×10^7	1.64×10^{11}	2.0×10^8	
3.61×10^7	1.39×10^9	2.0×10^9	
3.78×10^7	6.11×10^{11}	2.0×10^8	Some turbulence
4.31×10^7	1.67×10^9	2.0×10^9	No comment
4.55×10^7	1.72×10^9	2.0×10^9	Some turbulence
4.89×10^7	1.83×10^9	2.0×10^9	Some turbulence
5.4×10^7	1.89×10^{11}	2.1×10^7	Some turbulence
5.50×10^7	1.11×10^{10}	1.0×10^8	No turbulence
5.55×10^7	2.17×10^9	2.0×10^9	Some turbulence

TABLE I (CONT'D)

LAMINAR-TURBULENT TRANSITION DATA

Ra_a	Ra_ℓ	q_v	Remarks
6.11×10^7	6.66×10^{10}	5.6×10^7	No turbulence
6.66×10^7	1.17×10^{11}	2.0×10^8	Some turbulence
7.23×10^7	1.17×10^{11}	2.0×10^8	No comment
7.23×10^7	1.22×10^{11}	6.0×10^8	Very turbulent
7.23×10^7	1.22×10^{11}	6.0×10^8	No comment
7.23×10^7	1.22×10^{11}	6.0×10^8	No comment
7.23×10^7	1.28×10^{11}	6.0×10^8	No comment
8.34×10^7	2.89×10^{11}	3.1×10^7	Some turbulence
8.9×10^7	1.5×10^{11}	6.0×10^8	No comment
1.11×10^8	4.11×10^9	6.0×10^9	Very turbulent
1.11×10^8	1.89×10^{11}	6.0×10^8	No comment
1.17×10^8	4.44×10^9	6.0×10^9	Very turbulent
1.22×10^8	4.5×10^9	6.0×10^9	Very turbulent
1.22×10^8	4.56×10^{10}	6.0×10^9	Very turbulent
1.50×10^8	2.56×10^{11}	6.0×10^8	No comment
1.50×10^8	5.55×10^9	6.0×10^9	No comment
1.55×10^8	2.61×10^{11}	2.0×10^9	No comment
1.78×10^8	3.0×10^{11}	2.0×10^9	Some turbulence
1.78×10^8	3.0×10^{11}	2.0×10^9	No comment
1.89×10^8	3.16×10^{11}	2.0×10^9	No comment

TABLE I (CONT'D)

LAMINAR-TURBULENT TRANSITION DATA

Ra_a	Ra_ℓ	q_v	Remarks
2.44×10^8	4.11×10^{11}	2.0×10^9	No comment
2.78×10^8	4.7×10^{11}	2.0×10^9	Very turbulent
3.28×10^8	1.22×10^{10}	2.0×10^{10}	Very turbulent
8.34×10^8	4.39×10^{11}	1.1×10^{10}	No comment
1.05×10^9	5.55×10^{11}	1.4×10^{10}	No comment
1.17×10^9	6.11×10^{11}	1.9×10^{10}	No comment

The ability to predict the degree of turbulence in a given configuration is of great importance to the design engineer. A comparison of the experimental (essentially turbulent) results and the predictions of the laminar analysis show that there may be an improvement in Nusselt's Number by a factor of about two from turbulence.

7. Wall Heat Flux Distribution

It is predicted analytically that, for a uniformly distributed internal heat source, the wall heat flux will be a maximum at the top of the vessel and a minimum at the bottom for all of the axial wall temperature distributions investigated. This trend was confirmed experimentally. However, the data is only approximate. Wall heat flux values are inferred from the temperature differential across the test section wall. This differential was measured in the air-cooled tests as well as in the water-cooled tests. The axial variation of the coolant temperature of water cooled apparatus is much less than that of the inside wall surface so that coolant temperature can be considered almost constant. An error in estimating its gradient between the measured end points has little effect on the calculation of the temperature differential across the test section wall. Also the film coefficient on the outside of the wall is high because of forced convection, so that the temperature difference between wall surface and mixed mean coolant temperature at a given axial position is small. The resulting data, normalized to the wall heat flux at the axial midpoint, is presented in Figure 18 as a function of temperature differential ratio, (overall)/(fluid centerline to wall at top). This agress qualitatively with the analytical predictions (Figure 34). The experimental data covers only a range of points over the central 50% of the test section length. However, the analysis shows that the deviation of wall heat flux from the mean value is much greater at the ends. Reliable measurements near the ends were not possible. The test section wall thickness was not sufficiently small to substantially eliminate conduction, and there was uncertainty as to the quantity of heat flow from the vessel ends. Even though this were small compared to the total flow, it could affect the local temperatures quite significantly.

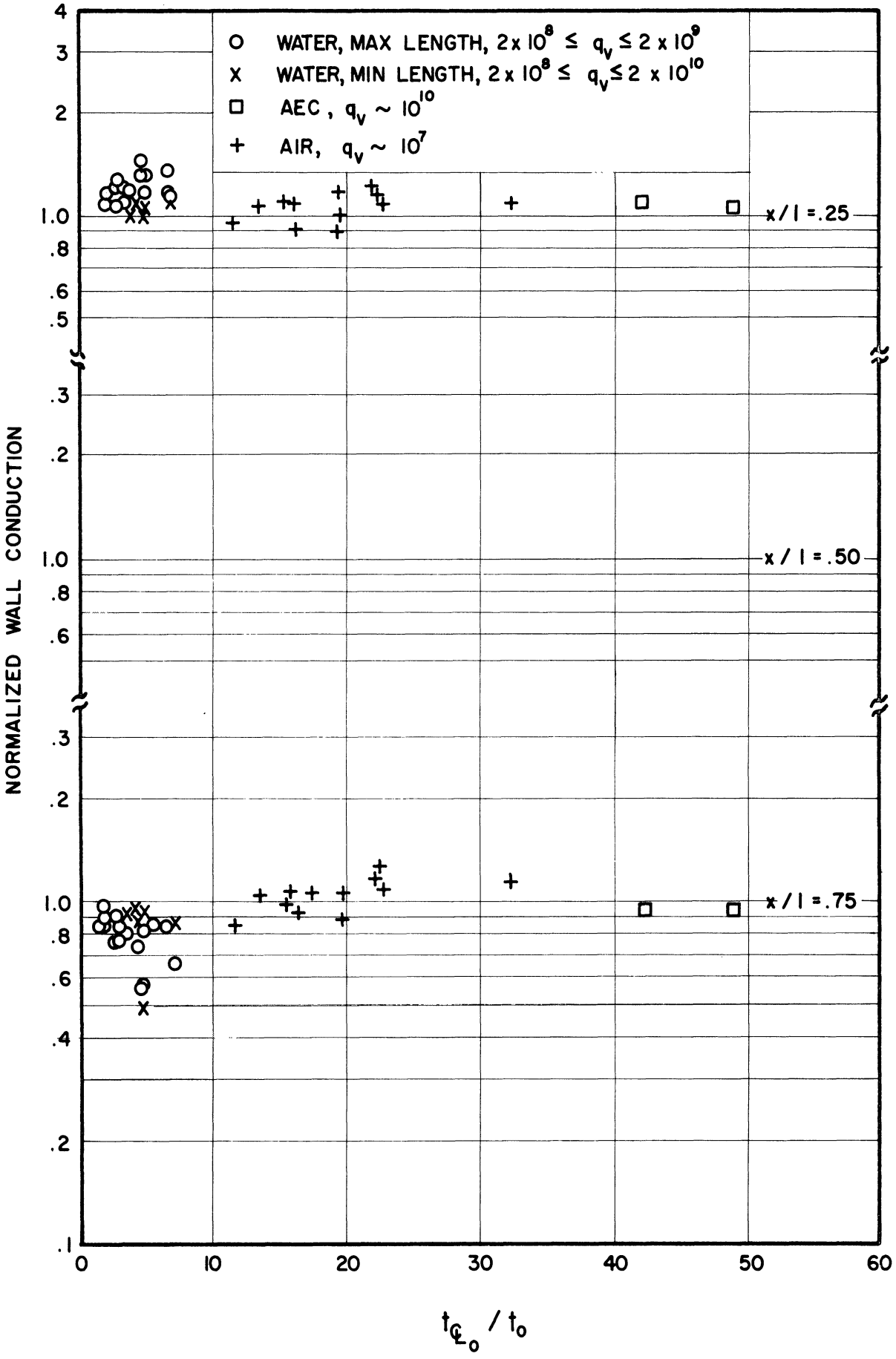

Figure 18. Normalized Wall Conduction vs. Overall/Radial Temperature Ratio Experimental Data.

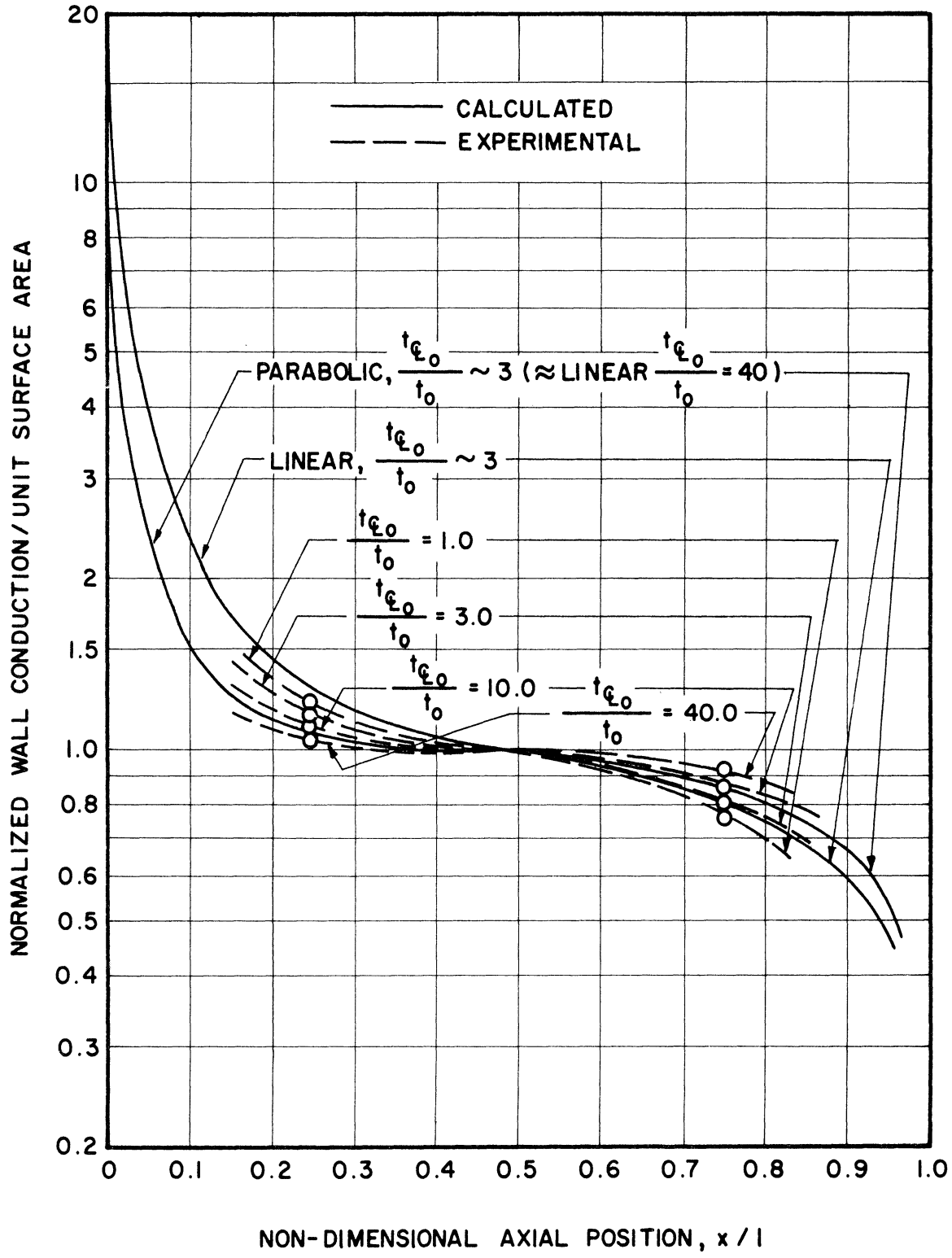

Figure 19. Normalized Wall Conduction vs. Non-Dimensional Axial Position, Linear and Parabolic Wall Temperature Distribution Comparison, Calculated and Experimental Data Comparison, Uniform Heat Source.

III. ANALYTICAL PROGRAM

A. General Approach

The general method utilized was patterned after that of Lighthill[6] in his analysis of a vessel with constant temperature walls and open at one end (closed at the other) to an infinite reservoir which is maintained at a temperature different from that of the vessel walls. Lighthill considered three possible flow regimes which covered the full range from infinite to small non-dimensional temperature differentials between infinite reservoir and wall. For the largest differential the postulated flow regime is of boundary layer type similar to that encountered with a flat plate in an infinite fluid. This has been extended somewhat into the range of lower differentials by considering the velocity in the core of the vessel which is of necessity of the opposite direction to that in the boundary layer. It was upon this particular approach that the analysis of the case of natural convection with internal heat source was based.

The details of the basic analysis used here have been given in previous papers.[1, 2] However, the general outlines will be repeated for convenience.

The vessel is considered to be composed of a multiplicity of discs normal to the centerline and of infinitesimal thickness. Boundary layer assumptions are made so that partial derivatives of the quantities parallel to the wall are neglected compared with those normal to the wall. Axial symmetry and steady-state are assumed. Integral relations for the conservation of mass, momentum, and energy, considering each disc as a control volume are written and non-dimensionalized by division with the proper terms. The conservation of momentum relation is further simplified by dropping the inertial terms with respect to those related to viscous shear. It was stated by Lighthill[6] and has been verified by the present work, that the assumption is reasonable if Prandtl Number is in the order of unity or greater, but is not defensible for fluids of very low Prandtl Number such as liquid metals. The only difference up to this point between the present analysis and that of Lighthill is that a volumetric heat source term is added to the energy conservation relation. Non-dimensionalization of this relation results in a non-dimensional heat source, q_v.

The general characteristics of the flow pattern are prescribed both on physical and theoretical grounds. The exact analysis of Pohlhausen and the experimental work of Schmidt and Beckman[12] and of Saunders[13] are

available for a vertical flat plate in an infinite fluid. It has been shown that the flow is of the boundary layer type and that velocity and temperature profiles extend approximately equal distances into the fluid if Prandtl Number is near unity. For the flat-plate geometry the solution has been evaluated out by numerical procedures for fluids of any Prandtl Number.[14] For those cases where the temperature differential is sufficient to cause the boundary layer thickness to be small, the circular tube differs to no significant extent from the flat plate. Furthermore, the predictions of Lighthill for his particular case have been largely verified experimentally by Martin.[15]

Considering all the above, it seems reasonable to assume that the flow pattern in the closed vessel will also be of boundary layer type, if the internal heat source is sufficiently strong. There will thus be a descending boundary layer along the wall and an ascending core along the vessel centerline. The temperature and velocity profiles will extend approximately equal distances into the fluid provided the Prandtl Number is near unity. Thus approximately unity Prandtl Number is required for two reasons.

Following Lighthill's procedure, velocity and temperature profiles were assumed such that at a given axial position the temperature increases parbolically from wall temperature to core temperature at the inner extreme of the boundary layer. It is assumed uniform across the core. A cubic relation is used for the velocity so that it varies from zero at the wall, through a maximum downward boundary layer velocity, and then upward to equality with the upward core velocity. This is assumed uniform at a given axial position. The point of tangency of boundary layer velocity and temperature profiles with the corresponding core values is defined as the inner extreme of the boundary layer (Figure 20). The assumed relations are reproduced below:

$$u = \begin{cases} -\gamma & \text{for } 0 < B < r \\ -\gamma\left[1 - \left(\frac{r-B}{1-B}\right)^2\left\{1 + \delta(r-1)\right\}\right] & \text{for } B < r < 1 \end{cases} \qquad (1)$$

$$t = \begin{cases} t(x) & \text{for } 0 < B < r \\ t(x)\left[1-\left(\frac{r-B}{1-B}\right)^2\right] & \text{for } B < r < 1 \end{cases} \qquad (2)$$

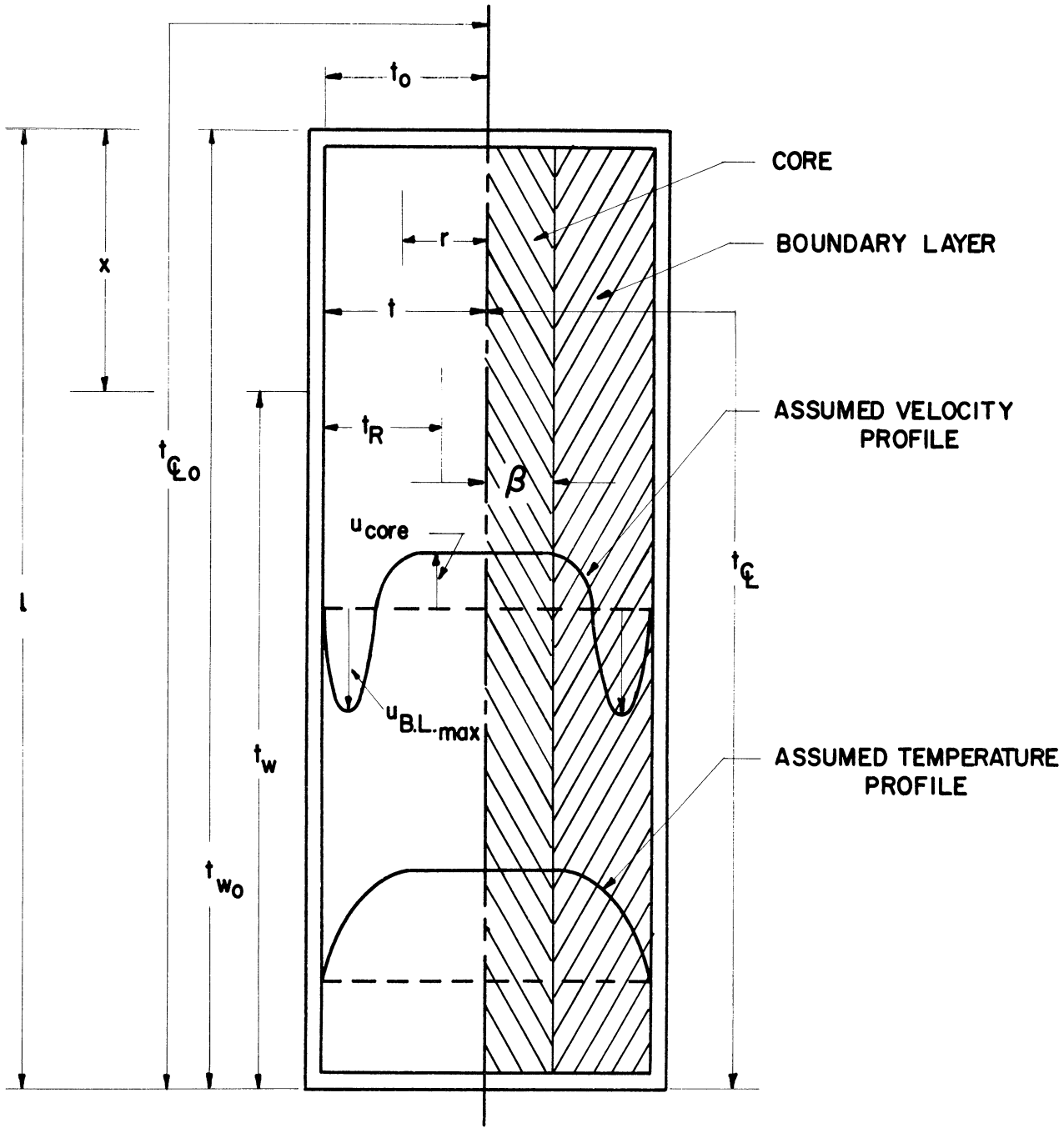

Figure 20. Test Section Nomenclature Schematic.

The assumed velocity profile is identical with that of Lighthill's. Because of the presence of the parameters γ and δ which are functions of boundary layer thickness, the magnitude and radial extension of the profile is left as a function of axial position. The temperature profile is also identical to Lighthill's except that the core temperature is considered to be a function of axial position rather than a constant as in Lighthill's case where there was no internal heat source. Then core thickness, β, is a function of axial position.

These profiles and their first derivatives obviously satisfy the conditions at the inner extent of the boundary layer and also at the wall. The first derivatives at these points are used to give wall heat flux and and wall shear in the energy and momentum relations. They are substituted into the integral conservation relations.

A further relation describing core temperature is required. This was not necessary in Lighthill's case where it was assumed constant. For the present analysis it was assumed that heat conduction would be negligible within the core and that the core temperature would be the result of the heat generation rate within the core and the time for which a portion of the fluid was exposed. Thus the axial gradient becomes proportional to the volumetric heat source strength and inversely proportional to the core velocity.

The core temperature relations result in two integral-differential equations, one representative of the core axial gradient and the other of the conservation of energy.[1] These relations apply individually to the radial discs into which the overall vessel is considered to be divided. The overall boundary conditions are:

1) Heat generation for the entire vessel must equal to the wall conduction for the vessel as a whole, i.e.: net energy convection for the entire vessel is zero.

2) Mixed mean boundary layer and core temperatures must be equal at either extreme of the vessel; i. e.: fluid leaving the boundary layer at the bottom is identical to that entering the core at that point. A similar statement applies at the top.

3) Boundary layer thickness at the top is zero since this is the point where the boundary layer starts.

As explained in previous papers,[1,2] the two independent integral-differential equations are written as difference equations, considering the vessel as a series of radial discs of small height, and the boundary conditions satisfied by an interative process using a high-speed digital computer. Since it is assumed that the vessel is composed of a finite number of discs, it is possible to consider different values of heat source strength and wall temperature for each disc so that the problem can be solved for arbitrary axial variation of wall temperature and heat source strength. However, no radial variations are possible. One of these possible variations is the Lighthill case. This is obtained by assuming that all the heat is generated in a thin radial disc at the bottom. Under these conditions the core temperature is constant as required.

B. Limitations of Method

When programmed for a high-speed digital computer, the method described above has a wide applicability since it is suited for completely arbitrary specification of wall temperature and heat source distribution. However, there are certain mathematical limits which have been explored. In some cases, before these are reached, some of the assumptions substantially lose their validity, so that a real limit of usefulness is imposed more quickly.

1. Axial Symmetry and Laminar Flow

In all cases the method is limited to axial symmetry and laminar flow. The latter is important since the experimental observations in the closed cell geometry indicate that a completely laminar flow may exist only with extremely low heat source strengths. For the case where the boundary layer hypothesis becomes questionable Lighthill considers the possibility of turbulence in his paper[6] but makes no analysis for the present range of interest. However, it is indicated that the existence of turbulence considerably increases the heat transfer. Murgatroyd[16] makes an analysis based on turbulent flow in a long cell containing a heat generating fluid. This is of great interest in itself but does not match the physical configuration considered in the present analysis, because Murgatroyd's cell is considered to be of infinite length to diameter ratio so that there is no transport of fluid between core and boundary layer except through the turbulent mixing (i.e.: no end effects).

2. Heat Source Strength and Wall Temperature Distribution

There are also limits upon the wall temperature distribution and the non-dimensional heat source strength, q_v. Since this involves the physical properties of the fluid, the dimensions of the vessel, and the volumetric heat source strength, the limitations are upon the combination of these rather than upon either length to diameter ratio or volumetric heat source considered alone.

Except through turbulence there is no apparent limit in the direction of high q_v since the solution becomes asymptotic to that of a flat plate in an infinite fluid as q_v is increased and the boundary layer becomes increasingly thin.

In the direction of low q_v there is a definite limitation when the boundary layer at some axial position occupies the entire cross-section of the tube. When this occurs no further boundary-layer development along with axial distance is possible and the limit of the solution has been reached (the prediction of a negative radius for the rising core results). The attainment of this limit depends upon the wall temperature distribution. It is shown by the envelope line of Figure 21 that this limit occurs for positive* wall temperature gradients in most cases at a q_v between 10^2 and 10^3. For negative** wall temperature gradients (Figure 22), it occurs at higher and higher q_v as the gradient becomes more negative. This range of values corresponds to very small volumetric heat sources easily attained in the laboratory, if the test section diameter is of the order of an inch. To a typical nuclear power reactors, this diameter is only about 1/16 of an inch. This lower limit on q_v is explored in detail in previous papers.[3,17]

The ratio of non-dimensional temperature differentials, t_{r_o}/t_o can also be considered a limiting parameter in combination with q_v as shown in Figures 21 and 22. A unity value for this ratio corresponds to a uniform wall temperature. Values greater than unity (positive wall temperature) imply a wall temperature gradient falling toward the bottom of the vessel and values below unity, indicate an opposite temperature gradient.

---

*Positive wall temperature gradient refers to cases where the wall temperature decreases toward the bottom.

**Negative to cases where it increases.

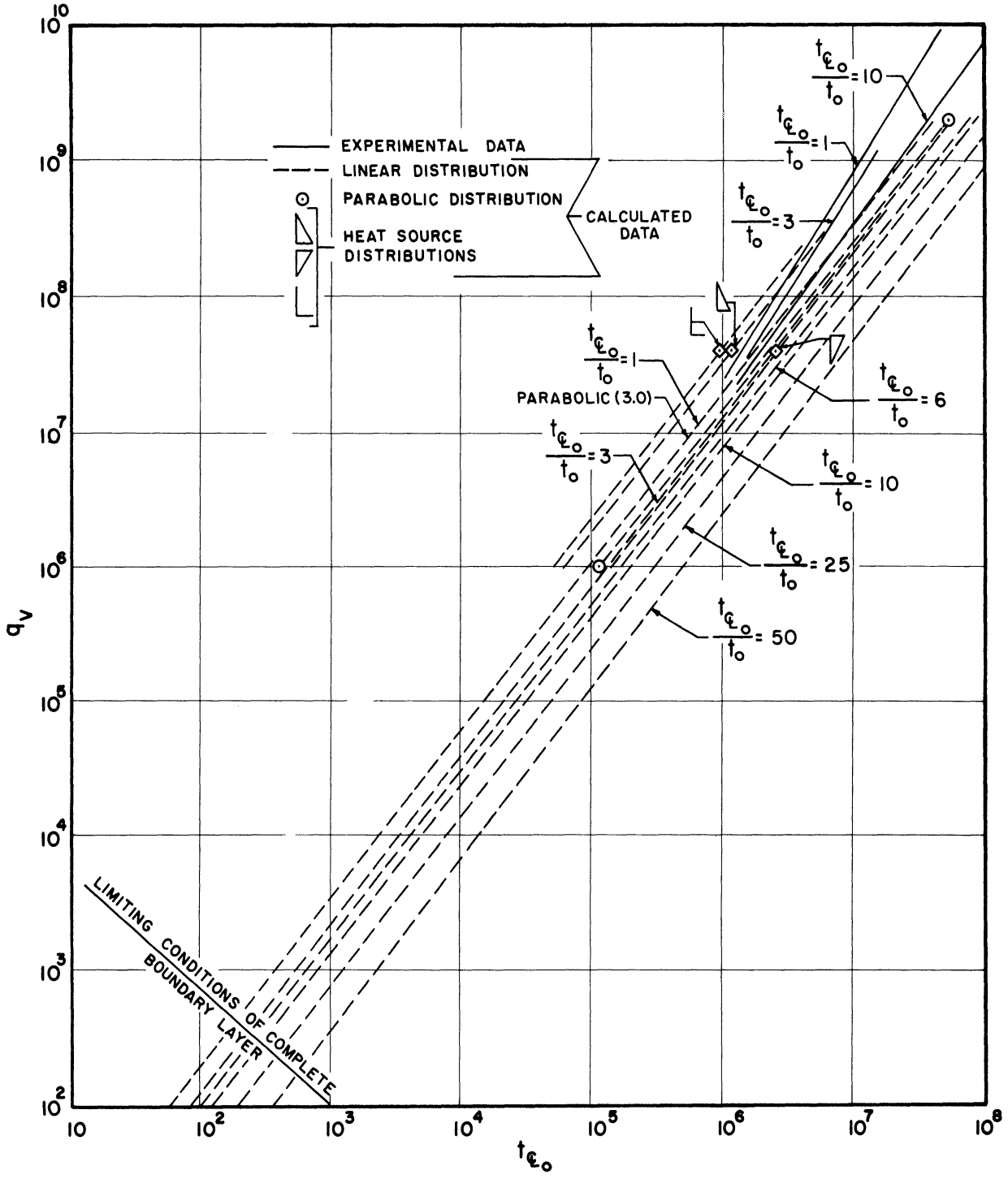

Figure 21. Non-Dimensional Heat Source vs. Overall Temperature Differential, Experimental and Calculated Data, Positive Wall Temperature Differential.

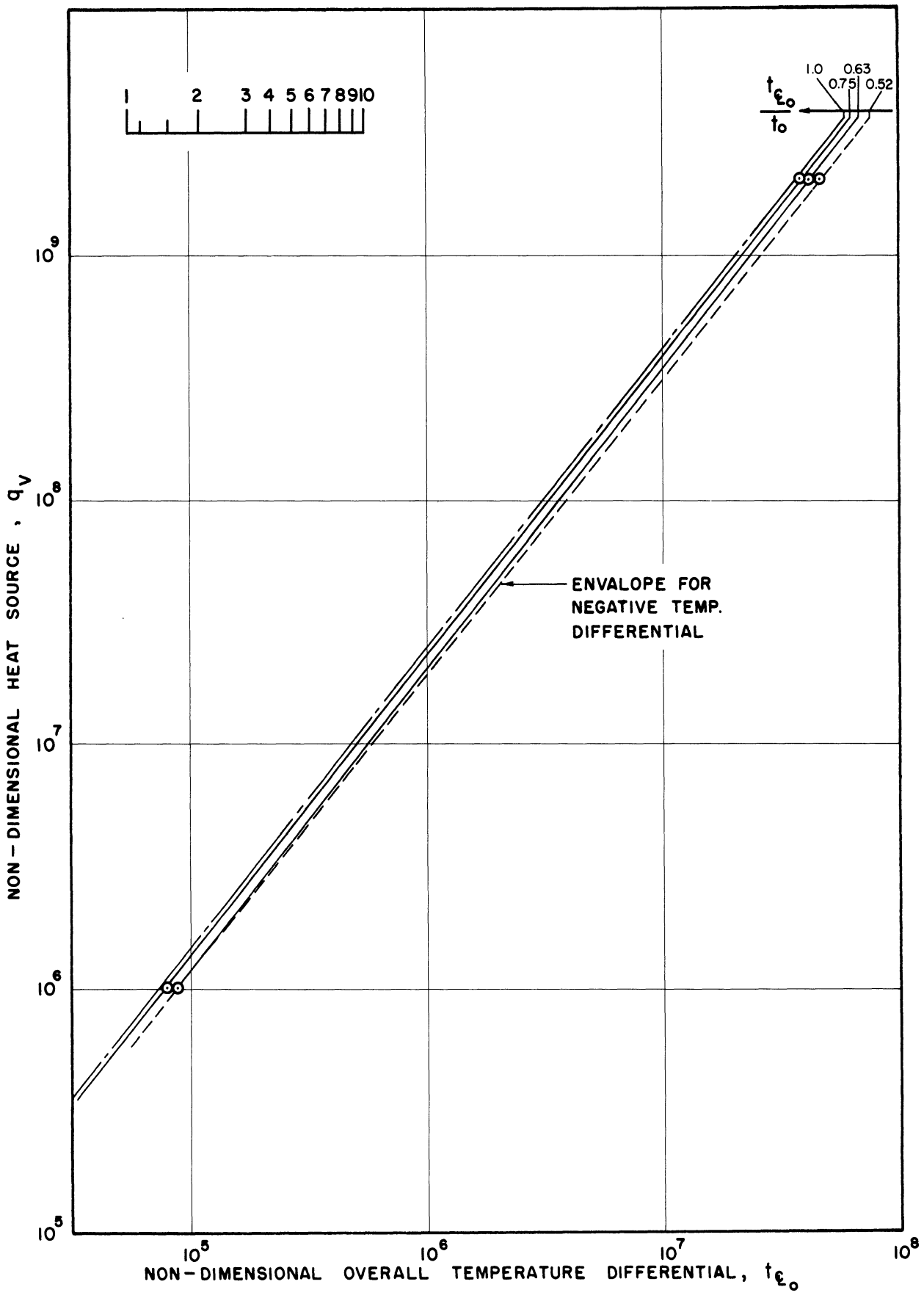

Figure 22. Non-Dimensional Heat Source vs. Overall Temperature Differential, Calculated Data, Negative Wall Temperature Differential.

With the experimental equipment on hand it proved impossible to impose such a gradient upon the test section inner wall. However, with a sufficiently small cooling stream directed downward in conjunction with a sufficiently strong internal heat source, it seems that such a gradient would be inevitable. In this case the boundary layer temperature would increase as it descended so that an apparently unstable flow pattern would result. Perhaps it would separate into various discreet circulating cells arranged axially rather than the single cell which has so far been observed.

The analysis yielded results over a rather limited range of these inverted wall gradients (i.e.: $t_{\ell_o}/t_o < 1$), as shown by the envelope curve in Figure 22. This curve is the division between cases where the core thickness is positive as physically required, and cases where the calculation shows negative core thickness. Its position is a function of both q_v and temperature ratio at all points. However, the dependence upon temperature ratio becomes much greater for those ratios less than unity. Over the range explored (up to $q_v = 2 \times 10^9$) the lowerst ratio for which a physically possible answer could be obtained was about 0.5. This limiting ratio increases as q_v decreases, and becomes unity at q_v of about 5×10^2.

The minimum overall temperature differential t_{ℓ_o}, for a given q_v, occurs at constant wall temperature where t_{ℓ_o}/t_o is 1. The calculation shows that either a positive or a negative wall temperature gradient results in a larger overall temperature differential.

There is no apparent mathematical limit in the direction increasing positive wall temperature gradients, and calculations have been made for t_{ℓ_o}/t_o values as high as 60. The effect of increasing the gradient is a dimunition of the boundary layer thickness for a given q_v, so that at high values of the ratio (about 40), the limiting q_v is reduced from about 2.5×10^2 to about 10^2.

Although from the viewpoint of the computer program, physically meaningful results can be obtained up to the envelope shown, the validity of some of the assumptions upon which the solution was based becomes quetionable as the limit is approached. The assumptions of temperature and velocity gradients concentrated in the boundzry layer and uniform across the core region becomes doubltful when the core occupies only a small portion of the vessel around the centerline. Because of these assumptions, for example, as the envelope is approached the analysis shows a core upward velocity considerably greater than the boundary layer downward velocity. However, this does not seem physically reasonable or in agreement with the observation.

Another limitation upon the validity of the solution at high wall temperature ratio is the assumption that heat conduction in the axial direction is negligible. Order of magnitude calculations show that this is reasonable in most cases since the gradient in the axial direction is small compared with the radial gradient near the wall where conduction is important. However, for very large wall temperature gradients this is not the case. Also, this assumption is least defensible for vessels with small length to diameter ratio since the end effects is more pronounced. For example, if the length/diameter = 10, boundary layer thickness /radius = 0.2 and t_{ℓ_o}/t_o = 20 the approximate ratio between radial gradient in the boundary layer and axial wall gradient would be

$$2 \times 10 \times \frac{1.0}{0.2} \times \frac{1}{20} = 5.$$

In this case the assumption of negligible axial conduction may be questionable. Further reduction of length to diameter ratio makes it more so. At this time, no information is available on the effect of this assumption on the overall results.

C. Coverage of Computer Solutions of Boundary Layer Solution

The computer solutions cover the range of q_v from 2×10^9 to about 10^2 (lower limit of applicability of solution) for t_{ℓ_o}/t ranging from about 0.5 (lower limit of applicability) to about 60. In general the investigation has been concentrated upon a uniform heat source distribution and linear wall temperature gradient. However, to afford comparisons over limited ranges, computations have been made for a half-cosine wall temperature distribution (Figure 23), since this resembles closely the experimental distributions, and also for various heat source distributions. These are described in detail in a later section.

D. Extension to Low q_v (Fully-Developed Region)

The lower limit of the boundary layer solution previously described is reached when, at some point within the vessel, the boundary layer has grown to the extent that it occupies the entire tube. In general, this occurs somewhere in the mid-portion of the tube, since the boundary layer thickness decreases in the extreme lower portion. If q_v values below the envelope shown in Figures 21, 22 are considered, a solution will result wherein the boundary layer grows from zero thickness at the top to a thickness equal to the radius at some point within the vessel. At this point the core thickness is necessarily zero and, according to this solution, becomes negative at points

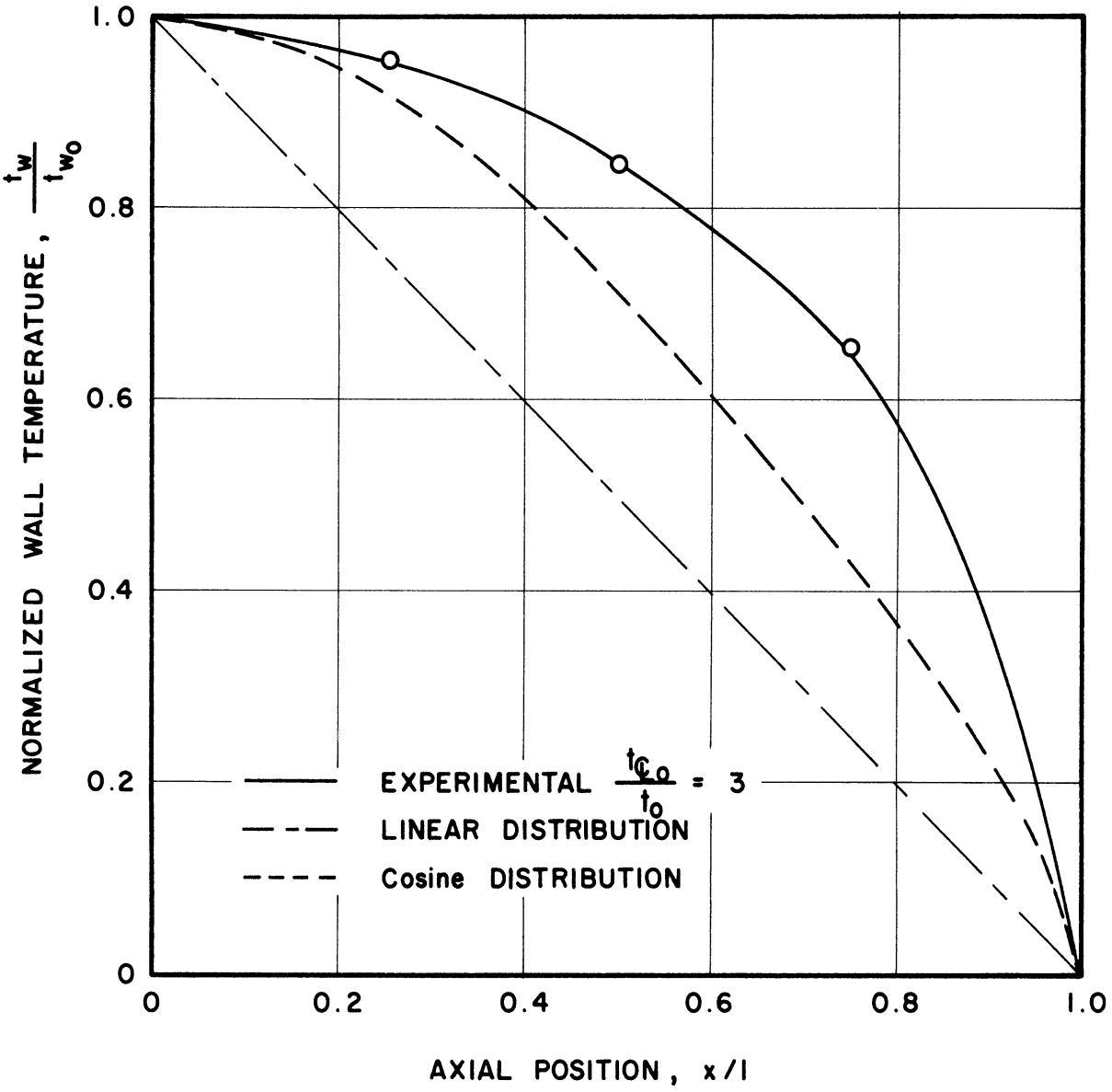

Figure 23. Various Wall Temperature Distribution.

lower along the axis. Thus the solution is physically meaningless below the point at which the boundary layer thickness becomes equal to the radius of the vessel.

For such a case a combined solution may be used. The original boundary layer solution is used for that portion of the vessel where the boundary layer is growing with axial distance. Below that point where the boundary layer fills the entire cross-section, it is considered to be of uniform thickness equal to the radius so that the flow becomes "fully developed" in the sense of pipe flow away from the entry section. A procedure similar to that of the original analysis can be used for this portion except that the boundary layer thickness is no longer a function of position but is constant. Details of the method are given in a previous paper.[3] A difference equation relating the non-dimensional temperature differentials, heat source and axial position can be derived which can be solved directly without iterative procedures. This "fully-developed solution" is then used for the lower portion of the vessel. It is easily shown[3] that in this portion, starting from the bottom of the tube, the non-dimensional temperature difference between wall and fluid centerline rapidly approaches $q_v/4$, a value that also applies to "rod flow"; i.e. : radial transport of heat by conduction only. Therefore, at the point of joining of the solutions, it is necessary that the boundary layer portion also gives a centerline to wall differential of this amount. A suitable solution for the boundary layer portion can be obtained by iteration to obtain this relation between core thickness and temperature differential. The solution for each portion individually assures that the conservation of mass, momentum, and energy are observed for planes normal to the axis at any axial position within that portion. Hence the combined soulution makes this assurance for the entire vessel, and also assures continuity of temperatures, wall heat flux, and velocities at the point of joining of the solutions.

The analysis for the "fully-developed" portion of the vessel is applicable both for constant and variable wall temperature, provided only that the axial temperature gradients are not large compared with the radial.[3] Regardless of the wall temperature differential between wall and centerline at any axial position in the fully developed portion is approximately $q_v/4$ as predicted by an analysis based simply on conduction theory.

E. Extension to Non-Steady State

It is believed that the steady-state analytical results so far achieved can be extended to the prediction of non-steady state heating and cooling rates of closed tanks by assuming that the flow regimes in such processes are a succession of quasi-steady states. Order of magnitude calculations of the time intervals involved indicate that this is not an unreasonable assumption. No numerical results of this type are as yet available.

F. Results of Computer Calculations

1. General Scope

For a given q_V and non-dimensional wall temperatures, t_w, specified at the centerline of each of the discs of the vessel considered, all other quantities are uniquely determined within the assumptions of the analysis. In addition to the overall heat transfer results, the computer program provides detailed information on local temperature, velocity, and heat flux.

2. Heat Source vs. Temperature Differentials

The overall non-dimensional heat source vs. non-dimensional temperature differential results are shown in Figures 21, 22 for the boundary solution. q_V is the ordinate and t_{ℓ_o} is the abscissa. This latter is measured from the fluid at the top of the vessel centerline to the wall at the bottom, and represents the maximum temperature differential existing in the fluid. The curve parameter, t_{ℓ_o}/t_o represents the proportionate strength of the wall temperature gradient in the positive direction.

Within the range of the solution, the curves appear as virtually parallel straight lines on the logarithmic coordinates. Because of this fact it is possible to formulate relations as below to represent the curves:

$$q_V = k\, t_\ell^n$$

The best values for these constants over the entire range investigated for

the curves of uniform heat source distribution and linear wall temperature gradients are given below (from Reference 17).

TABLE II

CONSTANTS FOR $q_v = k\, t_{\ell_o}^{n}$ for $10^2 < q_v < 10^{10}$

t_{ℓ_o}/t_o	k	n
1.0	0.921	1.22
3.0	0.314	1.24
10.0	0.0791	1.24
20.0	0.0357	1.25
40.0	0.0172	1.25

The exponent, 1.25, appears in the exact solution for the natural convection flow along a flat plate in an infinite fluid.

The temperature differential corresponding to a given heat source strength increases as the proportionate wall temperature gradient increases. However, as shown in Figure 18, the temperature differential at a given axial position between fluid centerline and wall actually decreases. This can be explained by the fact that the boundary layer thickness decreases as the proportionate wall temperature gradient increases and hence smaller fluid to wall temperature differentials are required across the reduced boundary layer to remove a given quantity of heat.

As q_v is reduced beyond the range of applicability of the boundary layer solution, the presentation of overall heat transfer results, in terms of ratio of temperature gradient, become less meaningful. Under this condition, the centerline to wall temperature differential becomes virtually a constant over most of the vessel length, increasing somewhat near the top and decreasing near the bottom. Its value over most of the vessel is simply $q_v/4$ and the overall differential, t_{ℓ_o} is controlled almost entirely by the wall temperature distribution. The increase at top and decrease at bottom becomes extremely local as q_v is reduced substantially

below the boundary-layer solution range. This is shown in Figure 24 where non-dimensional temperature differential, wall to centerline, is plotted against axial position for various q_v at constant wall temperature. The general character of the results for a positive wall temperature gradient and the fluid temperature follow the wall temperature in the same manner.

Returning to the boundary-layer solution (Figures 21 and 22), curves were run in addition to those previously described to determine the results of various non-uniform heat source distributions and of wall temperature distributions other than uniform gradients.

a. Heat Source Distributions

The heat source distributions listed below were investigated. In all cases the heat source was uniform for planes normal to the axis at a given axial position. All these computations are limited to the range of the boundary layer solution and constant wall temperature.

1) Constant volumetric heat source gradient from maximum at top to zero at bottom,

2) Constant volumetric heat source gradient from maximum at bottom to zero at top,

3) Sine distribution - zero at ends and maximum in center

Results are shown in Figure 21. The constant gradient distributions are signified by an inverted and an upright triangle respectively. These are listed below in the order of decreasing t_{E_o} necessary to remove a given heat quantity.

a) Constant gradient, maximum at bottom
b) Sine distribution,
c) Uniform distribution,
d) Constant gradient, maximum at top.

The relation of the constant gradients to the uniform distribution can be explained as follows: It is advantageous to add the major portion of heat near the bottom since the core temperature is increased by virtue of the heat addition. Hence, the mean temperature differential between fluid centerline and wall is increased and heat transfer is facilitated. The maximum difference in t_{E_o} due to the variation of heat source distribution is a factor of about 3.

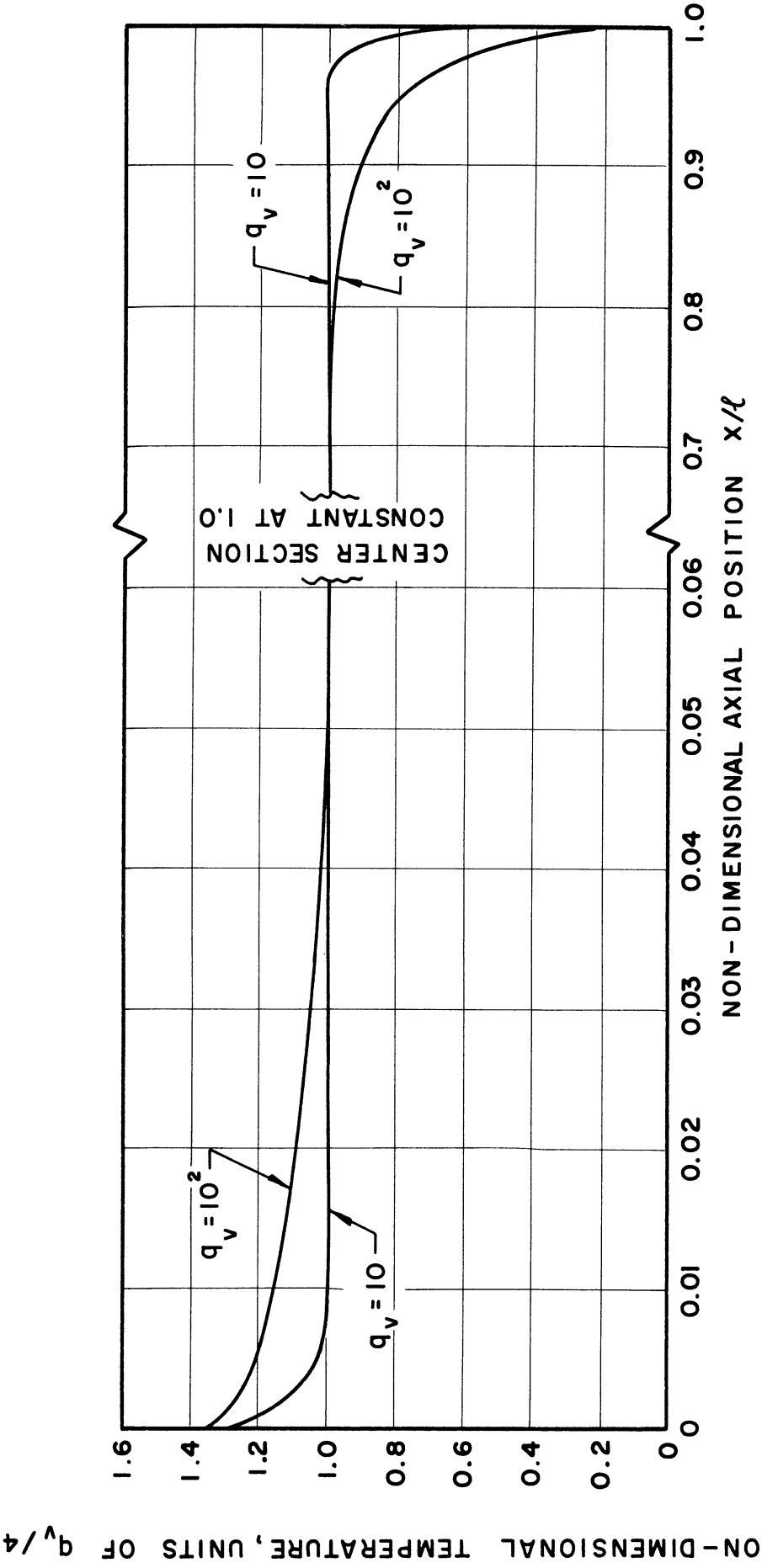

Figure 24. Non-Dimensional Wall to Centerline Temperature Differential vs. Axial Position, Fully Developed Flow Regime, Constant Wall Temperature.

Another heat source distribution was investigated. It was assumed that all the heat is added into a very thin radial plane (normal to the axis) at the bottom. This condition is analogous to the case of a vessel closed at the top and open at the bottom to an infinite reservoir maintained at a temperature greater than the wall temperature, and the volumetric heat source is zero. Since, for constant wall temperature, this is the case investigated by Lighthill,[6] it is possible to compare these results with his exact solution and also to investigate the effect of variable wall temperature.

It was found that the results obtained for constant wall temperature from the computer program were identical to those given by Lighthill. These are shown by the curve, $\llcorner$, in Figure 21. To compare with the results in the lighthill's paper, it is necessary to compute Nusselt Number from $Nu_a = q_v/2t_{\ell_o}$*.

In principle it is possible to use the program to compute results for the "Lighthill Case" with any desired wall temperature distribution within the bounds of applicability of the boundary layer theory. However, time has not been available to obtain these results within the present project.

b. Wall Temperature Distribution

The majority of the calculations consider either constant wall temperature or constant wall temperature gradient. However, the experimental results were taken with more or less parabolic distributions where the wall temperature is fairly constant near the top of the vessel and falls rapidly toward the bottom. Consequently a temperature distribution of this sort was run (half-cosine) to afford a comparison with the linear distribution of the same t_{ℓ_o}/t_o. As is shown in Figure 21, the overall heat transfer behavior is quite insensitive to the wall temperature distribution. It was also found that the local parameters were little affected.

3. Velocity

Figures 25 through 28 show the maximum boundary layer and non-dimensional core velocities resulting from the analysis over the full range of q_v, including both boundary-layer and fully-developed regions. Figure 25 for constant wall temperature applied to q_v from 2×10^9 to 10^6 for various heat source distributions. Their effect upon the magnitude

*t_{ℓ_o} is identical to Lighthill's t, in this case.

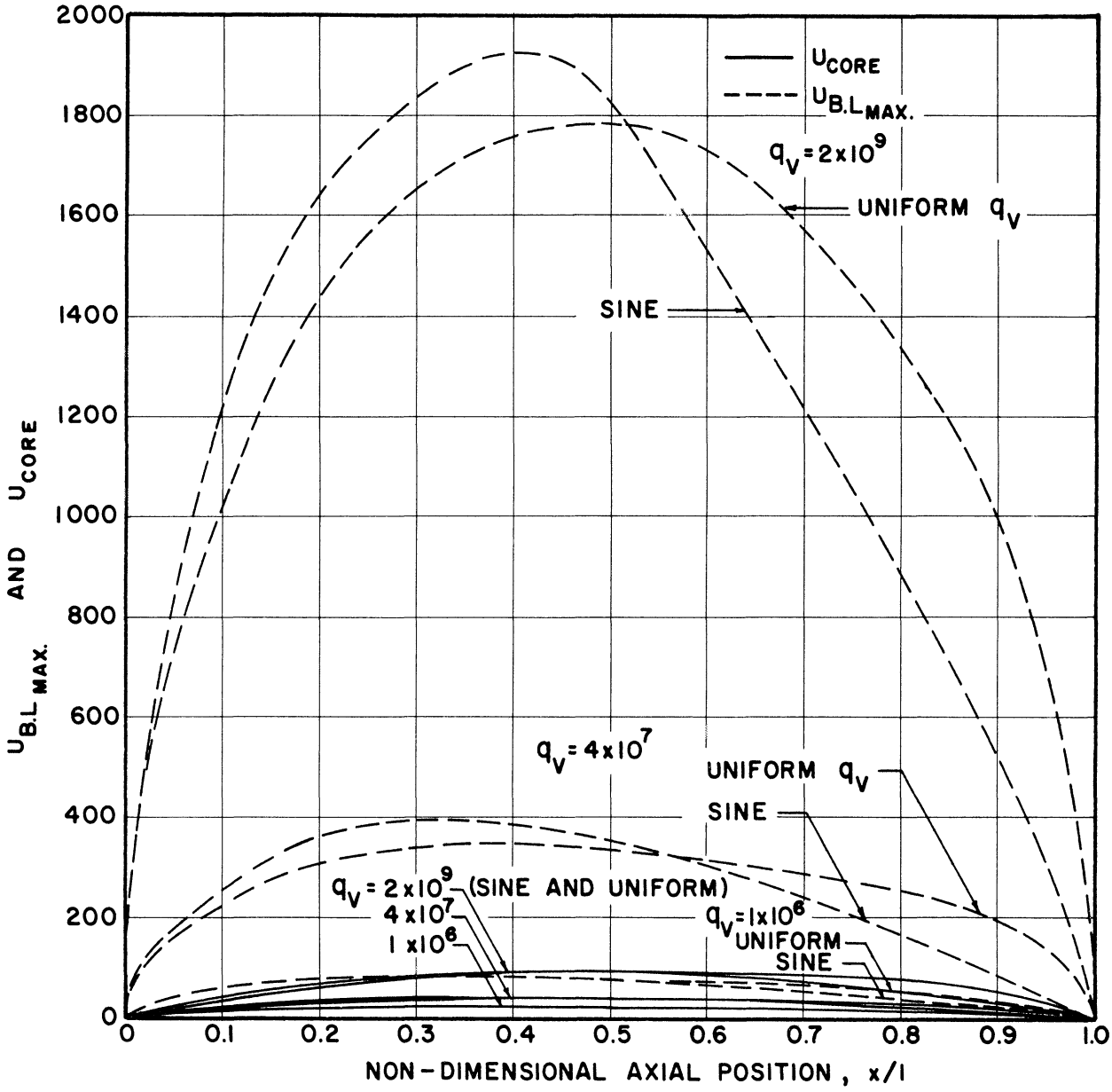

Figure 25. Non-Dimensional Core and Boundary Layer Velocity vs. Non-Dimensional Axial Position, Constant Wall Temperature, Comparison of Sine and Uniform q_v Distribution.

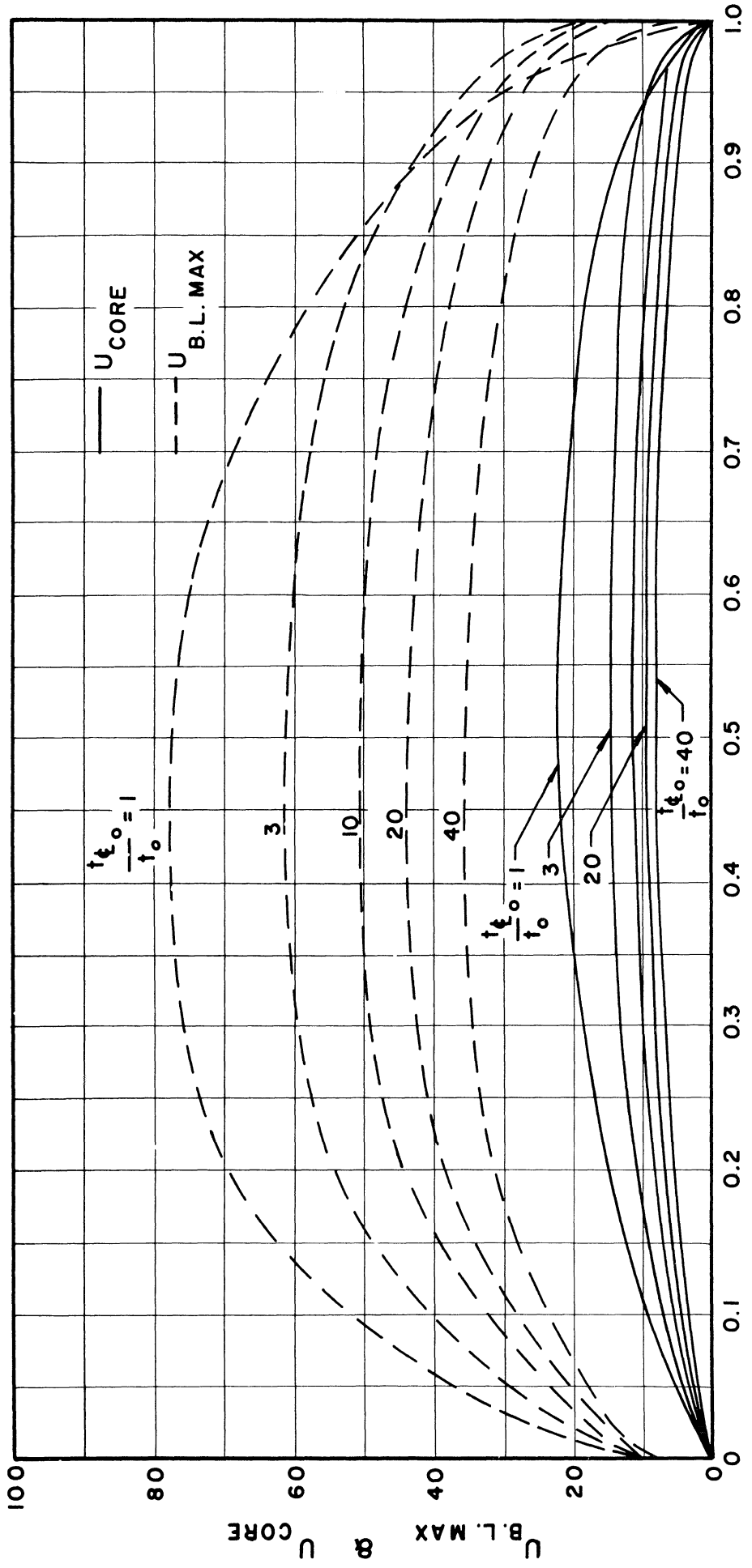

Figure 26. Non-Dimensional Core and Boundary Layer Velocity vs. Non-Dimensional Variable Linear Distribution of Overall/Radial Temperature, Uniform q_v.

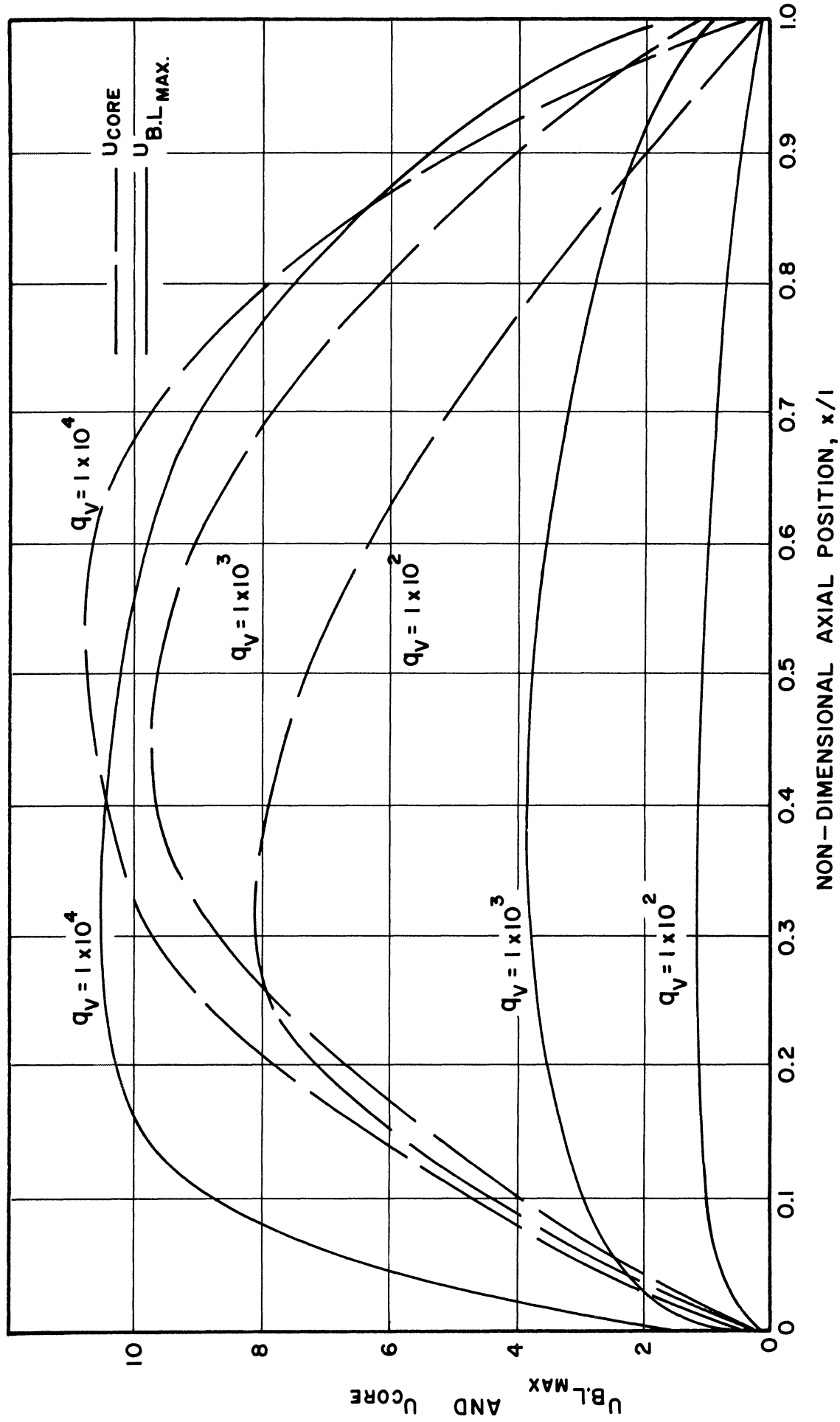

Figure 27. Non-Dimensional Core and Boundary Layer Velocity vs. Axial Position, Constant Wall Temperature.

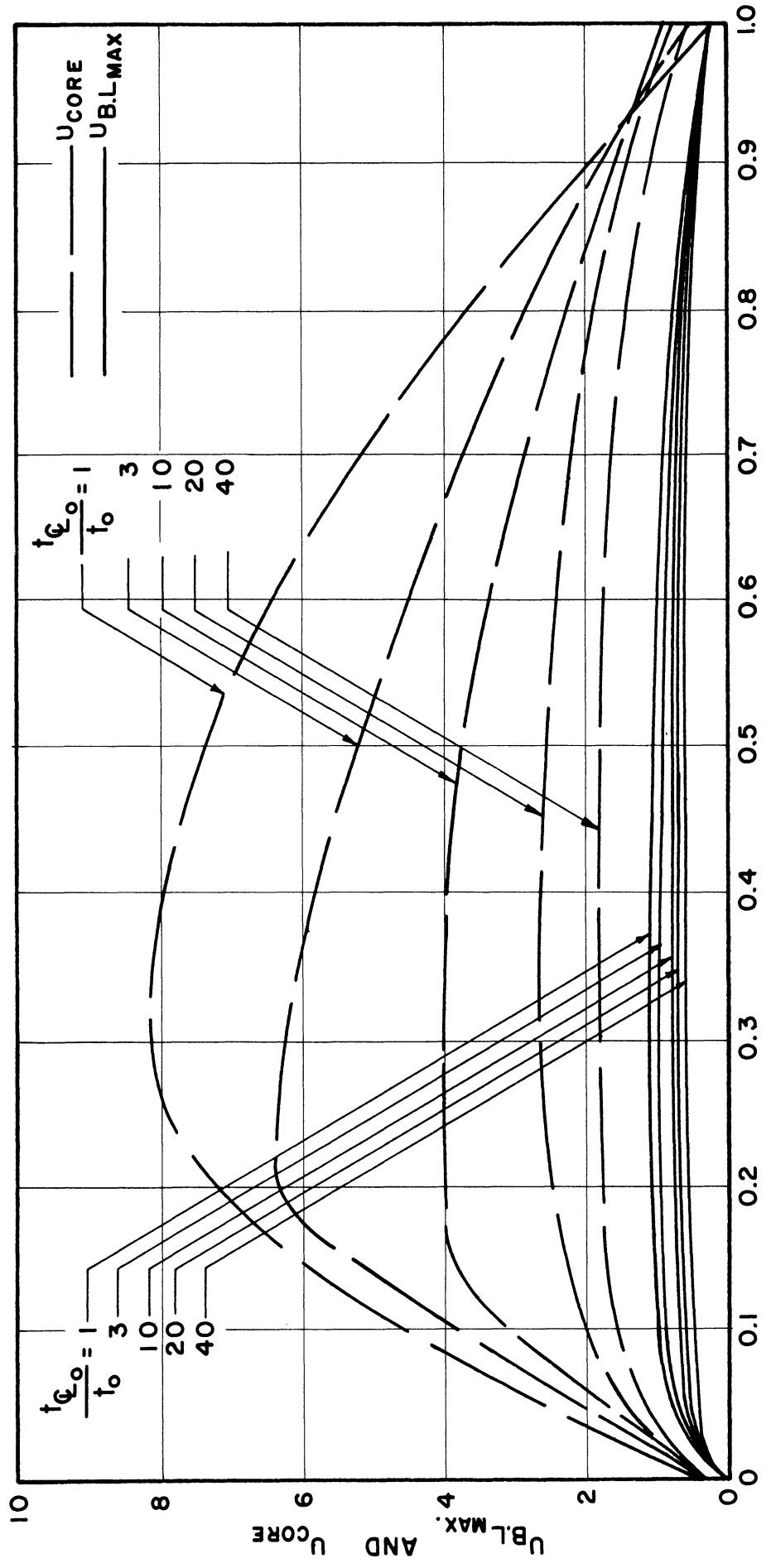

Figure 28. Non-Dimensional Core and Boundary Layer Velocity vs. Axial Position, Linear Variable Wall Temperature.

and distribution of velocity is not great. However, the velocity magnitude decreases by about the 0.5 power of q_v over this range and the ratio between maximum boundary layer and core velocity decreases by about the 0.1 power. In this q_v range, the boundary layer velocity is a factor of 3 to 4 greater than the core velocity, somewhat greater than the experimental factor (Figure 12). This factor decreases and reverses itself as q_v decreases.

Figure 26 shows the effect of wall temperature gradient upon the velocities at a given q_v. It is noted that the effect of increasing wall gradient is a reduction of velocities.

Figure 27 shows boundary layer and core velocities at constant wall temperature in a lower q_v range (10^2 to 10^4). As q_v is continually decreased, the results show that the core velocity eventually becomes greater than the boundary layer velocity (the factor is about 5 at $q_v = 10^2$).

Figure 28 shows the effect of wall temperature gradient for low q_v. Again, increasing gradient reduces velocity. The q_v range covered by Figures 27 and 28 is the lower end of applicability of the boundary layer solution and also includes the fully developed regime ($q_v = 10^2$ curve).

Anticipated velocity profiles for infinitely long tubes with both laminar and turbulent flow are given in the literature.[14] These cannot be presented in the framework of the present analysis because infinite length implies $q_v = 0$.

4. Boundary Layer Thickness

In the range of application of the boundary layer solution, the boundary layer is assumed to start from zero thickness at the top of the vessel. The analysis shows a very rapid growth near the top followed by a leveling off to a thickness which is maintained approximately throughout most of the length. The mathematics of the solution is such that the boundary layer thickness falls very steeply near the bottom also to zero. However, the predicted behavior at the vessel ends is probably not physically significant. The flow model employed is one-dimensional, and cannot accurately predict the flow pattern in the vessel ends where cross-flow must predominate.

Figures 29 and 30 show typical boundary layer thicknesses plotted against axial position in the high q_v range. The effect of variable wall temperature and variable heat source distribution is also shown.

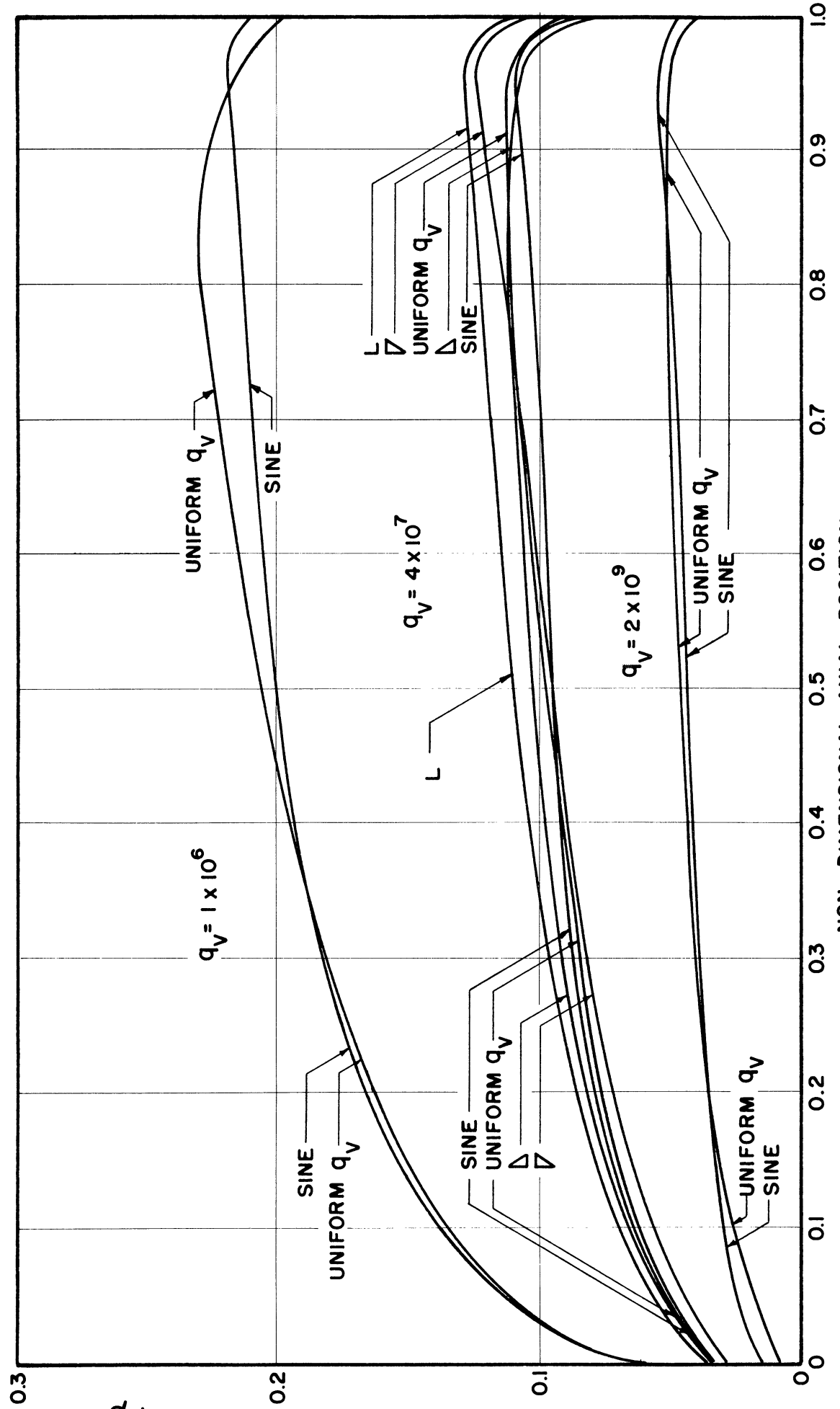

Figure 29. Non-Dimensional Boundary Layer Thickness vs. Non-Dimensional Axial Position, Comparison of Various Axial Heat Source Distribution.

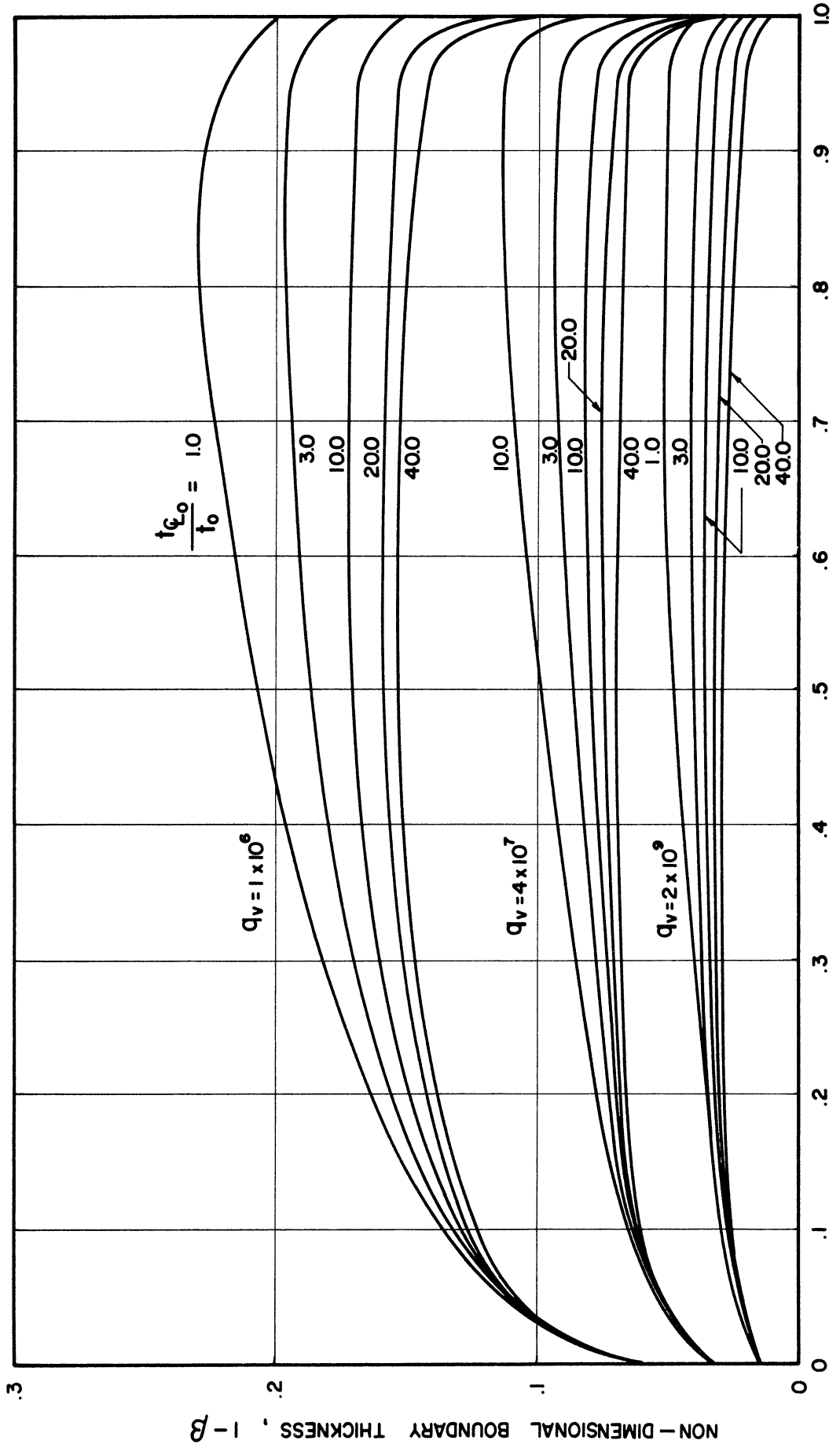

Figure 30. Non-Dimensional Boundary Layer Thickness vs. Non-Dimensional Axial Position, Uniform Heat Source Distribution.

Figure 31 shows similar results for low q_v above and below the boundary-layer solution level of Figure 21. The curve for $q_v = 10^2$ is plotted as computed from the machine program showing negative core thicknesses over a major portion of the vessel. Hence it is not physically meaningfull.

Figure 16 shows the comparison between analysis and observation.

5. Wall Heat Flux

In many physical applications the distribution of wall heat flux is of great importance since it controls the temperature differential across the vessel wall. This is limiting in some nuclear power reactor designs because of the corresponding thermal stresses. Also, knowledge of its distribution is necessary to the solution of a problem. Suppose, for example, the heat source strength and distribution and also the coolant inlet conditions and flow rate are known. In this rather typical case the wall heat flux is a coupling parameter between the heat balance equations and consequent temperature rise of the coolant, and, via the wall differential, is the internal wall temperature distribution. A trial and error solution could be made whereby the heat flux distribution is assumed, the coolant temperature distribution can be calculated, and then the internal wall temperature distribution is obtained. If, per data of the sort herein given, the assumed heat flux distribution is consistent with the calculated internal wall temperature distribution and the known heat source distribution, the problem would be solved.

In all cases the analysis shows an increase of wall heat flux toward the top of the vessel and a decrease toward the bottom, even for those cases where the heat source is predominently in the lower portion (as the "Lighthill case"). The results in the high q_v range are plotted in Figures 32, 33, and 34 showing the effect of variation of heat source strength, distribution, and wall temperature distribution. The sharpness of the rise at the top and the decrease at the bottom is increased by a reduction of q_v or an increase in proportionate wall temperature gradient.

Similar results for the low q_v range (above and below the limit of the boundary layer solution) are shown in Figures 35 and 36. The trends mentioned above persist. For very low q_v, the wall heat flux is virtually constant over most of the tube (for uniform heat source distribution) but shows a sharp peak at the top and drop at the bottom. However, these deviations from the mean are extremely local, covering only a few percent of the length for $q_v \leq 10^2$. Such local peaks may not be of physical significance. They would induce axial heat flow in the wall which would reduce the otherwise predicted wall differential in this region.

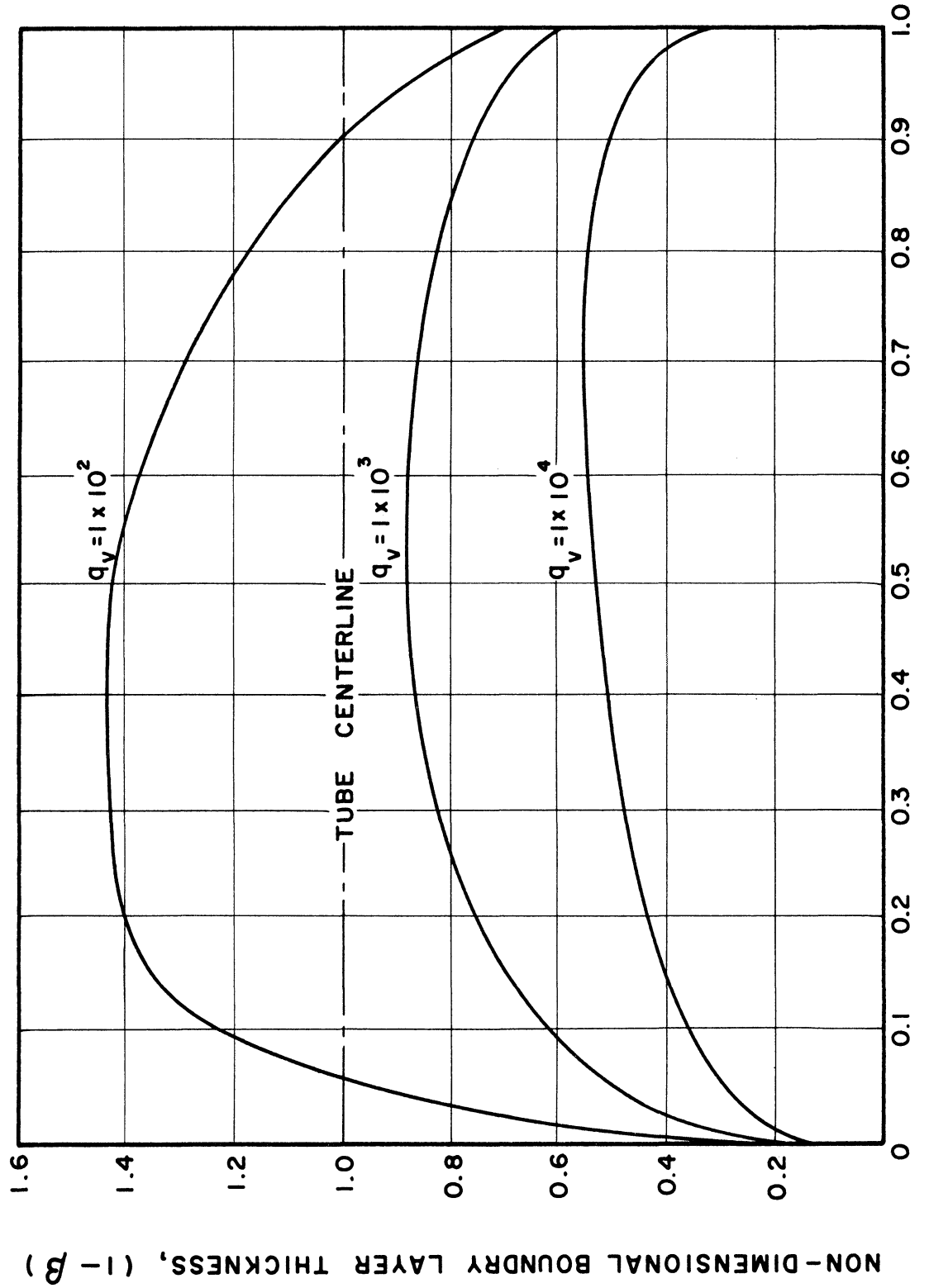

Figure 31. Non-Dimensional Boundary Layer Thickness vs. Axial Position, Constant Wall Temperature.

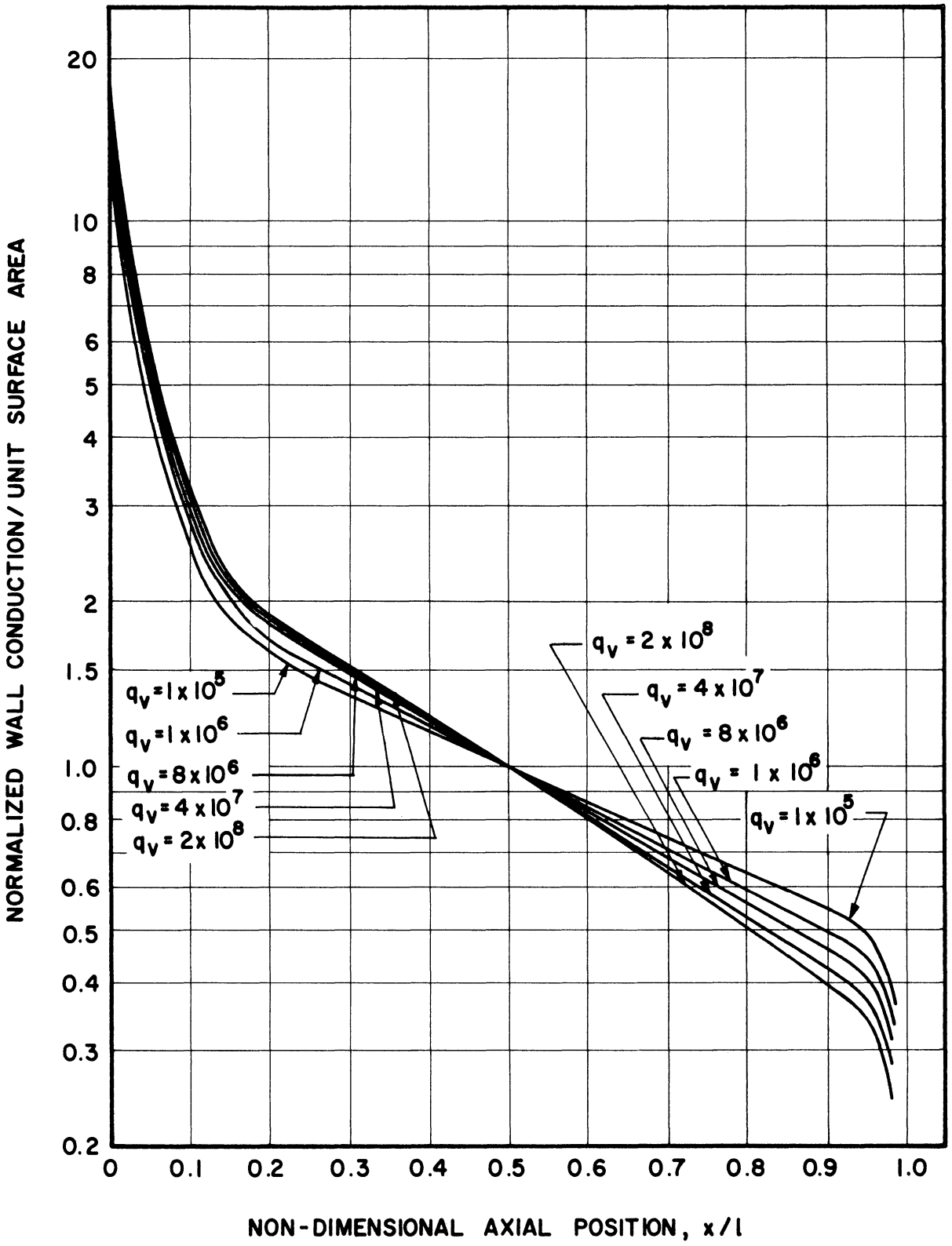

Figure 32. Normalized Wall Conduction vs. Non-Dimensional Axial Position, Constant Wall Temperature, Uniform Heat Source Distribution.

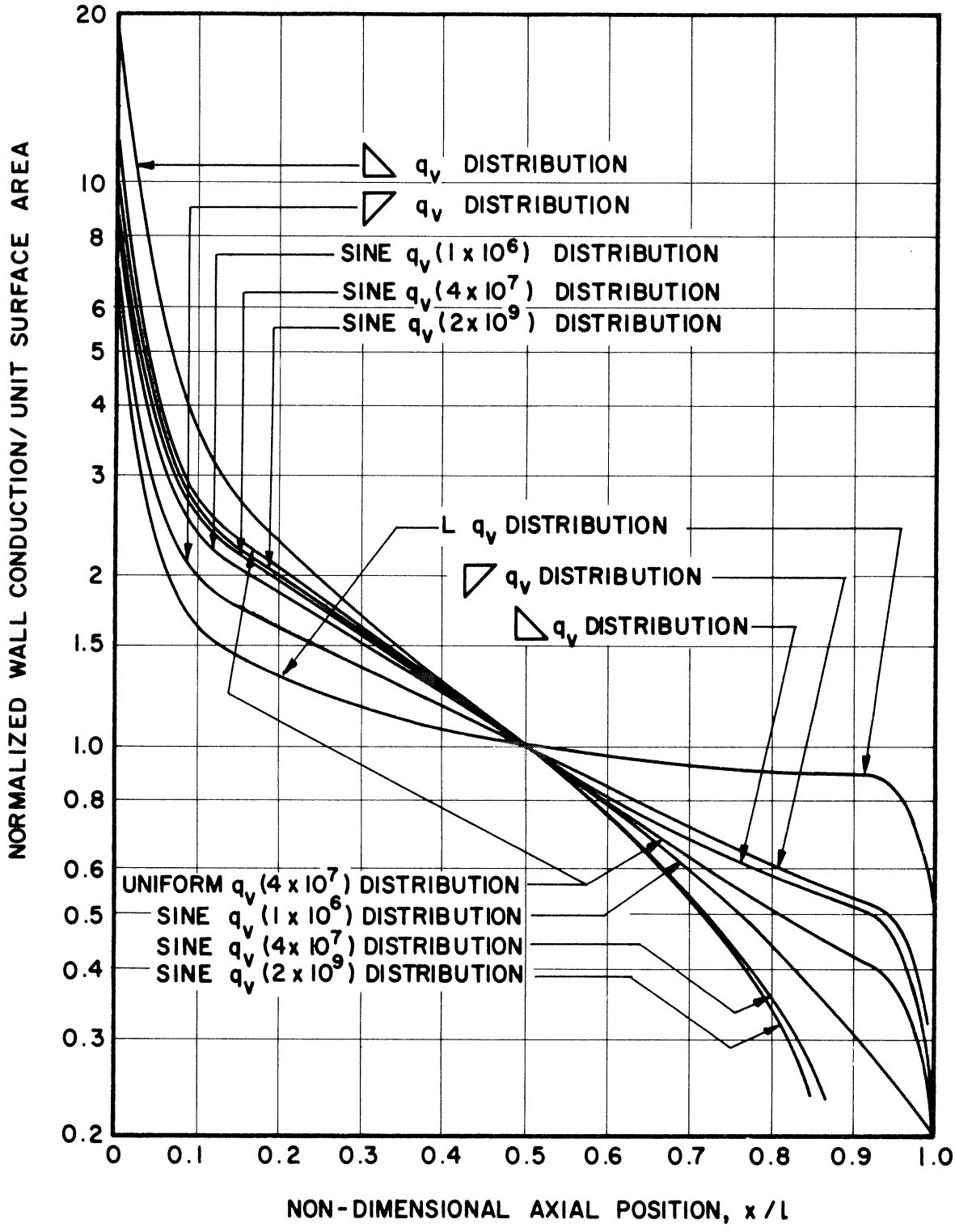

Figure 33. Normalized Wall Conduction vs. Non-Dimensional Axial Position, Constant Wall Temperature, Variable Axial Heat Source Distribution.

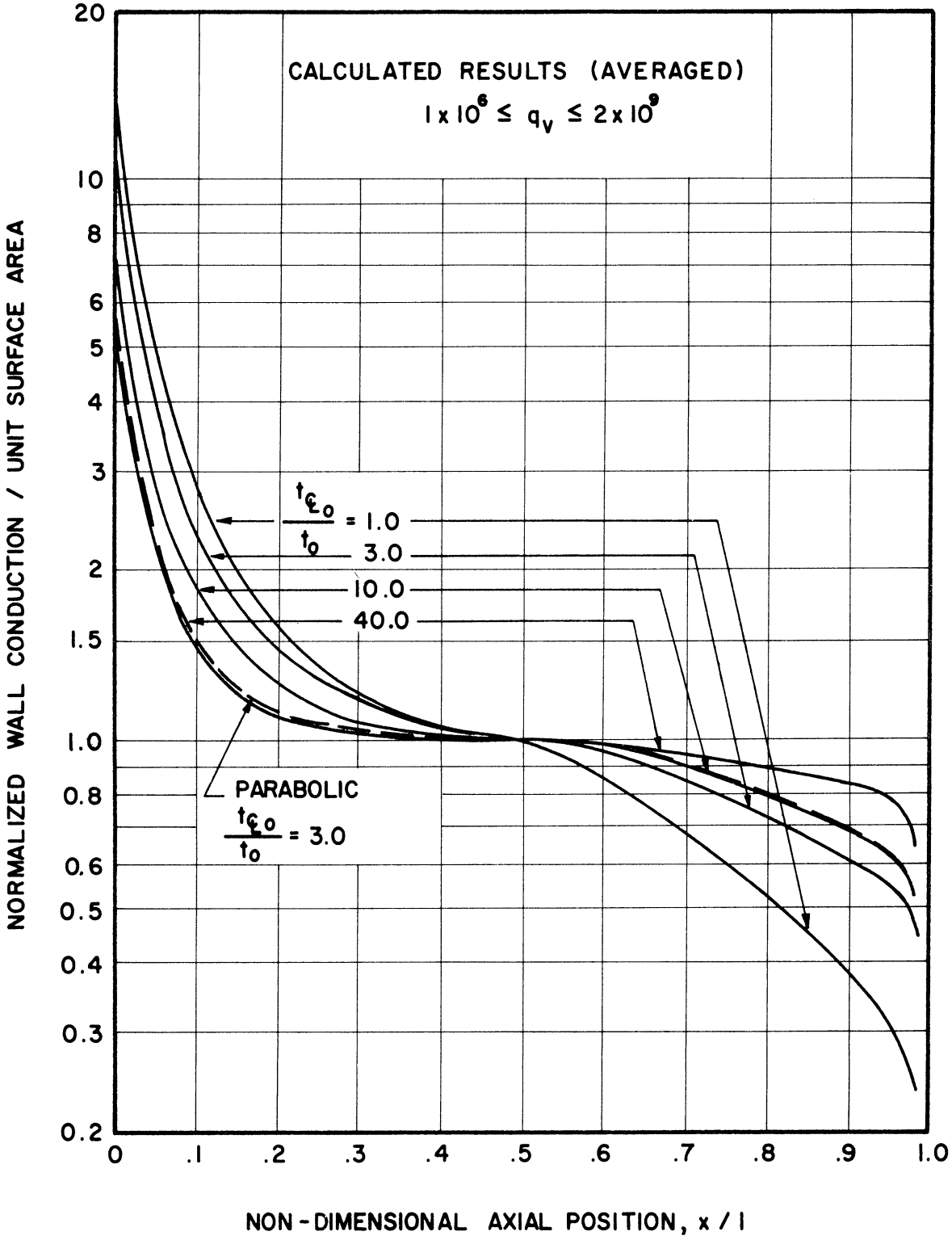

Figure 34. Normalized Wall Conduction vs. Non-Dimensional Axial Position, Linear Wall Temperature Distribution, Uniform Heat Source.

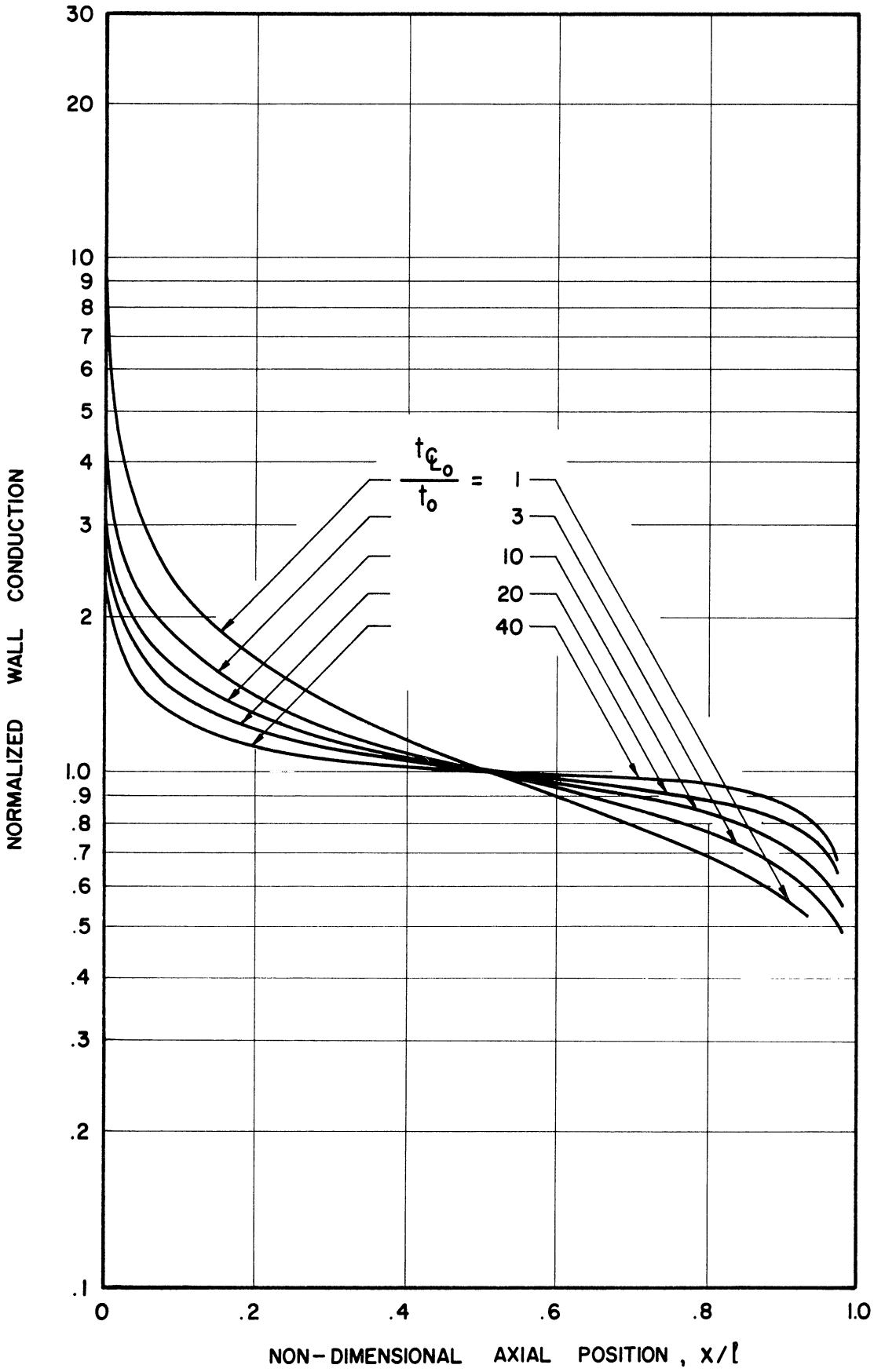

Figure 35. Normalized Wall Conduction vs. Non-Dimensional Axial Position, Linear Variable Wall Temperature Uniform Heat Source.

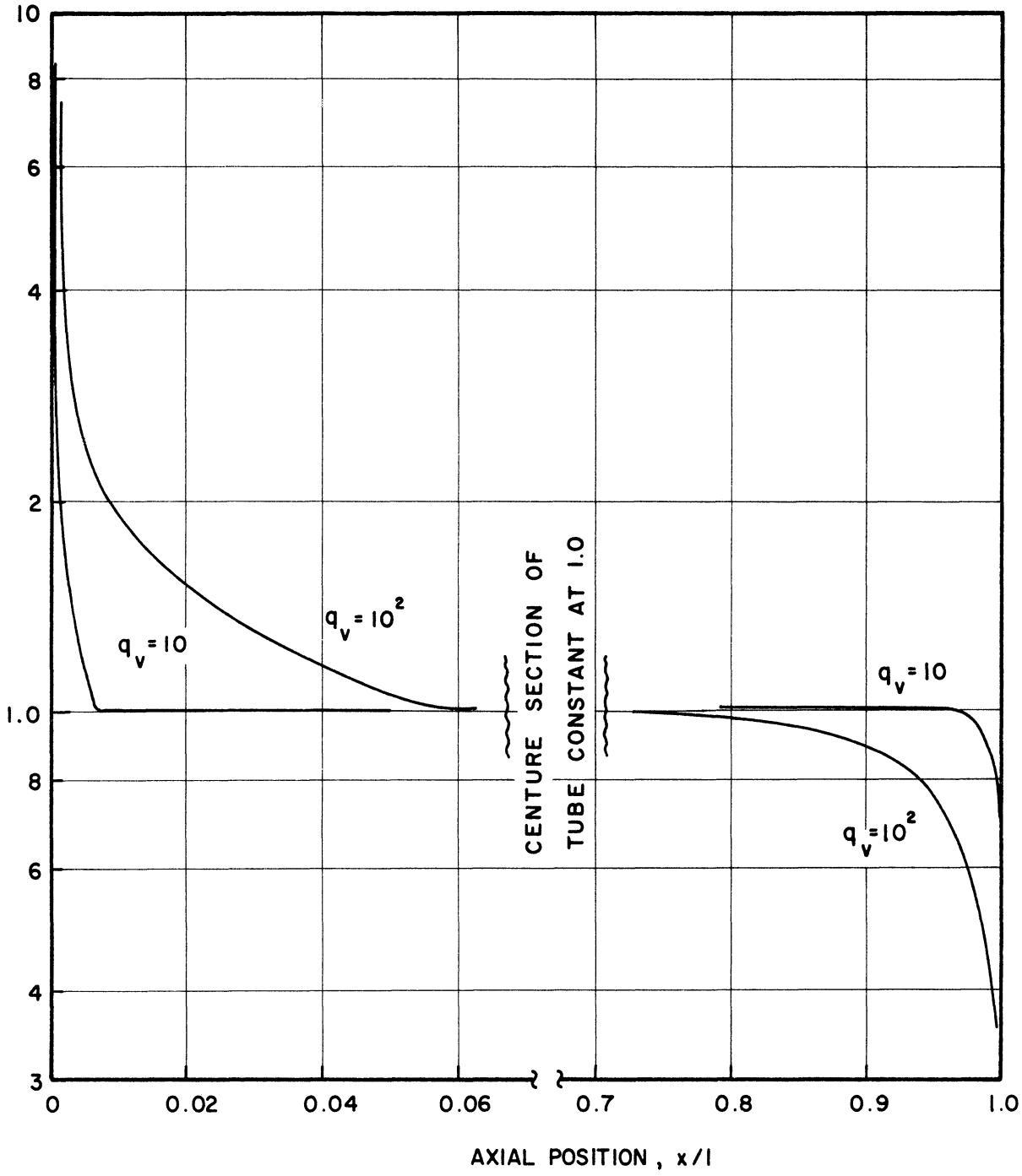

Figure 36. Normalized Wall Conduction vs. Axial Position, Constant Wall Temperature, Uniform Heat Source, Fully Developed Flow.

Since the temperature differential between fluid centerline and wall is at a maximum at the top and the boundary layer thickness is at a minimum, the radial temperature gradient at this point is increased. Hence, the greatly increased heat flux at the top for a uniform internal heat source distribution is expected.

Figures 35 and 36 consider the only uniform q_v distribution in lower range. However, heat transfer for this range of q_v where the flow pattern is fully developed over most of the vessel is substantially as predicted by conduction. Hence the wall heat flux distribution would closely follow the internal heat source distribution, with the exception of the extremely local variations at the ends which were previously discussed.

G. Comparison with Experimental Observations

Order of magnitude agreement between the predictions of the laminar flow analysis and the experimental non-laminar observations exists with respect to velocity, boundary layer thickness, and wall heat flux distributions. These comparisons are illustrated in the previous figures.

The most important point of comparison (Figure 21) is between the overall temperature differentials for a given non-dimensional heat source and wall temperature distribution. The experimental temperature differentials are in all cases less than those derived from the laminar analysis. It is presumed that this is primarily a result of turbulent mixing in the actual case.

Aside from the effect of turbulence, the assumption of a single mean temperature as applying to the entire vessel seems a likely cause of significant discrepancy. Because of the large temperature dependence of viscosity, the temperature differences were such that a typical viscosity variation from minimum to maximum within the test section might be as much as 20%.

The factor between experimental and analytical, non-dimensional temperature differentials is approximately 0.5 for the high q_v range and 0.9 for the low range. It is felt that if this type of analysis is used for a different configuration, heat source strength, or wall temperature

distribution, these approximate factors can be applied to give at least an engineering estimate of the temperature differentials to be expected. Also, the detailed comparisons given for wall heat flux distribution, velocities, and boundary layer thicknesses can be used as a guide for the desired quantities.

IV. CONCLUSIONS

The experiments described provide a wide range of data for the engineering evaluation of a physical system consisting of a vertical cylindrical vessel, closed at the ends, with internal heat source. Coolant and heat source distribution must be axially symmetrical.

The laminar flow analysis allows a further extrapolation of these data to conditions other than those covered by the experiments. In addition it should allow an extension into the problem of unsteady-state heating and cooling of closed vessels.

BIBLIOGRAPHY

1. Hammitt, F. G. ASME Paper No. 58-SA-30.

2. Hammitt, F. G. ASME Paper No. 58-A-212.

3. Hammitt, F. G. and Brower, E. M. University of Michigan Research Institute Report, IP-340.

4. Brower, E. M. Master Thesis, Nuclear Engineering Dept., University of Michigan, 1958.

5. Yip, S. Master Thesis, Nuclear Engineering Dept., University of Michigan, 1959.

6. Galbraith, D. Master Thesis, Nuclear Engineering Dept., University of Michigan, 1959.

7. Quarterly Journal of Mechanics and Applied Mathematics, 6 , (1953), pp. 398-439.

8. Hartuett, J. P., Welgh, W. E, ASME Paper 56-A-113.

9. Siegel, R., Norris, R. H. ASME Paper No. 56-SA-5.

10. Poppendick, H. F., Palmer, L. D. Nuclear Science and Engineering, 3 , No. 1, (Jan, 1958).

11. Mohr, D. Master Thesis, Nuclear Engineering Dept., University of Michigan, 1958.

12. Schmidt, E. and W. Beckman, Tech. Mech. Thermodynamics, 1, (1930), pp 34-39 and 391-406.

13. Saunders, O. A. Proc Roy. Soc. A-157 (1936), pp 278-91.

14. Murgatroyd, W. ED/R 1559. Atomic Energy Research Establishment. Harwell Berks, England, 1954.

15. Martin, B. W., Cohen, H. Brit. Journal Applied Physics, 5 , (March, 1954) pp. 91-95.